2006

Analysis of photonic crystal defects for biosensing applications

Naveen Kumar Paturi
West Virginia University

ANALYSIS OF PHOTONIC CRYSTAL DEFECTS FOR BIOSENSING APPLICATIONS

Naveen Kumar Paturi

Thesis submitted to the
College of Engineering and Mineral Resources at
West Virginia University
in partial fulfillment of the requirements for the degree of

Master of Science
in
Electrical Engineering

Committee members:
Dr. Lawrence A. Hornak, Ph.D., Committee Chairperson.
Dr. Dimitris Korakakis, Ph.D.
Dr.Aaron Timperman, Ph.D.

Lane Department of Computer Science and Electrical Engineering
Morgantown, West Virginia
2006

Keywords: Biosensor, Photonic Crystal, E-beam Lithography

ABSTRACT

ANALYSIS OF PHOTONIC CRYSTAL DEFECTS FOR BIOSENSING APPLICATIONS

Naveen Kumar Paturi

Photonic Crystals (PCs) have been the subject of intense study from their inception. These structures provide precise control of optical transmission properties through the choice of their periodic lattice parameters and materials with which they are fabricated. The sensitivity of optical properties of photonic crystals to the changes in refractive index at one or more lattice sites makes these structures potentially very attractive devices for developing a biosensor. Very small changes in the refractive index of one or more defect sites can be sensed accurately using these nano size structures. This work deals with the modeling and theoretical evaluation of the sensitivity of PC defect transmission states to the changes in refractive index of single and cluster defects. The band gap shifts as a function of the change in different parameters for a 2-D triangular lattice of holes in silicon and GaN were explored. The shifts in the optical transmission with change in refractive index of one to seven defects were calculated using MPB (MIT Photonic Bands) and Optiwave FDTD tools and analyzed. Efforts defining the fabrication process for PC structures were also outlined. Optimization of E-beam lithography to write these patterns in PMMA was also demonstrated. Patterns of 200nm radius with lattice constant of 500 nm in PMMA 495 A2, and patterns of 300nm radius with 1 micron lattice constant were optimized in PMMA 950 A4.

Acknowledgements

I would like to thank Dr.Hornak, my advisor, who has been a source of inspiration in my pursuit of Masters degree. I would like to thank him for his patience, support and encouragement through out the research. I would also like to thank my other committee members Dr.Korakakis, and Dr.Timperman for their support throughout my research. I sincerely acknowledge Dr.Kolin Brown for his support in the lab. I would also like to thank Dr.Lederman, Debin Li for their help with E-beam lithography, and Dr.Liviu Magean, Steve Carpenter and Adrienne Macleod for their assistance with SEM images. Special thanks to Sridhar for his support with sputtering and RIE. I would also like to thank my family for their support and encouragement.

Contents

List of Figures

List of Tables

CHAPTER I

INTRODUCTION

1.1. Biosensors

One area which has a huge impact on our daily lives is the area of biosensors. The increasing threat posed by bioterrorism, and the constant increase in health concerns has increased the demand for rapid detection and identification of bio molecules. Optical biosensors are attracting interest in recent times since they have the potential for rapid sensing and detection of bio molecules. Remote sensing, high selectivity, high sensitivity and real time monitoring are some of the advantages of optical biosensors. A biosensor in general has two important components, 1. Detection mechanism and 2. Transduction mechanism [1]. The general principle of biosensor operation is described in the figure 1.1.

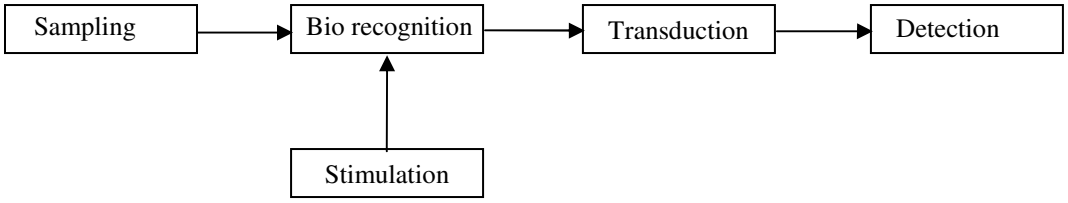

Figure 1.1 General scheme of biosensing [1]

The sampling unit introduces the analyte into the detector. The bio recognition element binds with a specific element providing the bio detection specificity [1]. Stimulation can be any type of external field that produces a response. For optical biosensors, the external stimulation is the optical field. The transduction unit transforms the response produced by the bio recognition unit into a specific signal detectable by the detector unit. So an optical biosensor in general uses the changes in the frequency (or wavelength), polarization, or amplitude caused by the recognition element in the presence of external stimulation, and then this change is detected. There are different kinds of optical biosensors like fiber optic biosensors [2], waveguide biosensors [3], and evanescent wave biosensors [4]. A

novel type of biosensor, which is recently making rapid progress, is the photonic crystal biosensor.

1.2. Photonic Crystals

Photonic crystals are novel fabricated materials, which are orderly arranged dielectric media [5, 6]. Intense research is going on to develop a photonic crystal biosensor, which offers many advantages like high sensitivity and selectivity. Photonic crystals basically are lattice structures, with variation in refractive index in 1, 2 and 3 dimensions. This variation in refractive index causes the wave propagating through the structure to undergo interference, such that there is a band gap for specific wavelengths if the structure is properly designed. Creating defects can confine particular optical modes which are otherwise not allowed. This unique property of photonic crystals can be exploited in developing a biosensor. Photonic crystals offer precise control over the light propagating through them. Defects can be created by change in refractive index, size and shape of either one or more lattice sites. The defects can be filled with fluid, gas or biomolecules, and the interaction of light with these materials can produce changes in the transmission/reflection properties of the crystal, which can be detected. An adequate number of nano scale binding events can initiate refractive index change at a lattice site and create a point defect. The optical properties of photonic crystals are very sensitive to the changes in the refractive index of defect sites. These events can be initiated in a cluster of defects (super defect) [7], to enhance the optical emission. The 2-D Photonic Crystal structures which contain sub micron level periodic structures in a high refractive index material are suitable for detecting the nano scale binding events, with very small sampling volumes. Given the integration of these structures with suitable detectors, sources, and micro fluidics can be done, photonic crystal biosensors can become an integral component of lab-on-chip architectures.

1.3. Prior work and motivation

From the inception of the concept of photonic crystals, a large body of work has been done to develop the theoretical models and fabrication methods to use the crystal properties for many applications. Literature shows that 2-D photonic crystals can

be effectively used as biosensors. The shift in resonant wavelength of a point defect, as the function of surface refractive index is practically shown by E.Chow etal [8]. The change in transmission properties with wave guide defects, initiated by absorption of light by DNA in the defects is theoretically modeled [9]. The delivery of the sample into these nanoscale defects can be challenging. The integration of these structures with micro/nano-fluidic channels provides a platform to effectively control the volume of samples to be delivered into the defect cavities [10]. The refractive index of the samples at specific sites can be manipulated by different mechanisms and the change in emission can be controlled and efficient biosensing can be done with high sensitivity. This research works deals with understanding the basic properties of photonic crystals, exploration of their defect behavior for use in biosensor applications, and development of basic PC fabrication techniques. Dependence of optical properties of these crystals on different materials at different wavelengths is also studied. This work also explores through simulation the variation of emission properties as a function of defect refractive index. This work also includes analysis, design and modeling of various parameters to optimize the emission from the defects. Steps towards fabricating 2-D photonic crystals with these design parameters also will be discussed.

1.4. Organization of thesis

Chapter II of this thesis reviews the fundamental principles of photonic crystals and explains how the light is propagated within these structures. This chapter also outlines the basic photonic crystal defect mechanisms explored here for biosensing. Chapter III investigates the use of photonic crystals in the infrared region and deals with design of parameters for the 2-D Photonic Crystal. The chapter also explains modeling and simulation tools used and discusses the results of simulation. Chapter IV deals with the fabrication procedure for fabricating a 2-D Photonic Crystal and the fabrication process determined as part of this work is outlined. The work is summarized and recommendations for future directions are discussed in Chapter V.

CHAPTER II

PHOTONIC CRYSTALS

2.1 Introduction

Photonic crystals are orderly arranged dielectric media, with length scales comparable to the wavelength of interest [5], [6]. These structures are the optical analogue of semiconductor crystals. The periodic arrangement of refractive index gives a periodic potential to light flowing through it, thus giving rise to band gaps and allowed gaps in the dispersion relation. As a result, light with specific energy is allowed or blocked in specific directions. By changing the geometry, size, shape and refractive index of the lattice, we can create defects thus creating intra band modes, which are not present in otherwise perfect crystal. By manipulating the geometry of the crystal, we can control several properties of light propagating through the medium of periodically varying refractive index. If the refractive index contrast is high enough, and the absorption of light by material is minimal, then scattering at the interfaces produces the same effect for photons as the periodic potential in semiconductor produces for electrons [5]. These interfaces act like Bragg like reflectors. Intentionally created defects give rise to localized electromagnetic states in the band gap. These defects may be of two types Point like defects, giving rise to resonant cavities, and line defects which act as waveguides. The change in these optical properties can be used to create various effects, which can be applied for various applications like high 'Q' Lasers [11], LEDs [12], bio and chemical sensors [8, 9, 10], switching circuits [13], waveguides with sharp bends [14], optical interconnects [15] and many more.

2.2 Analogy between Semiconductors and Photonic crystals

As stated earlier, photonic crystals are the optical analogue for semiconductors. The various effects that photons undergo while propagating through a Photonic Crystal (PC) are very similar to that of electrons in semiconductors, so it is important to see the similarities and differences between electrons and photons. Both electrons and photons are elementary particles that simultaneously exhibit particle and

wave type behavior. The similarities in characteristics of photons and electrons are summarized in the following table [16].

Photons	Electrons
Wave length	
$\lambda = h/p = c/\upsilon$	$\lambda = h/p = h/mv$
Eigen Value (wave) Equation	
$\nabla \times [(1/\varepsilon(r)) \nabla \times H(r)] = (\omega/c)^2 H(r)$	$H\psi(r) = (h^2/2m)(\nabla . \nabla + V(r)) \psi(r) = E \psi$
Interaction Potential in a medium	
Dielectric Constant (Refractive index)	Coulomb Interactions
Propagation through a classically forbidden zone	
Photon tunneling (Evanescent wave) with wave vector, k, Imaginary and hence amplitude decaying exponentially in the forbidden zone.	Electron-Tunneling with the amplitude (probability)decaying exponentially in forbidden zone.
Localization	
Strong scattering derived from large variations in dielectric constant (Refractive index)	Strong scattering derived from a large variations in Coulomb

Table 2.1. Analogy between photonic crystals and Semiconductor crystals [16]

2.3 Types of Photonic Crystals

In photonic crystals, refractive index varies spatially in specific directions. Depending on how many dimensions this spatial variation of refractive index is in, we

classify photonic crystals as 1-D, 2-D, and 3-D. So a 1-D photonic crystal is one which has periodic variation of refractive index in only one direction. The simplest possible PC is the well known quarter wave stack, which has alternating bilayers of different refractive index materials [17]. Light of specific Wavelengths when incident on this is completely reflected. If the spacing is perfectly right, light scattered at layer interfaces interfere destructively inside the material. This acts as a mirror. A 2-D Photonic Crystal consists of alternating layers of dielectric materials, with variation in 2 dimensions. These can be of two types, air rods in a dielectric medium and dielectric rods in air. Similarly 3 –D Photonic Crystal have the variation in all 3 different directions. These offer a complete band gap to light. As a result, light of any polarization for any angle of incidence can be manipulated. Fabrication of 2D PC samples is relatively easy compared to that of 3D PCs. Moreover calculations of band structures are also far easier. Although a full band gap doesn't exist in a strict sense, 2D Photonic Crystal slabs are important from the view point of both academic and application uses. For 2D PCs, the dimension 'h', the height, perpendicular to the propagation of wave is very large compared to the lattice parameter 'a'. For the Photonic Crystal Slab (PCS), 'h' is comparable to 'a' or wave length (λ). The periodic variation causes the Bragg like reflections in 2-dimensions along the plane and total internal reflection guides the wave propagation in the third dimension (i.e.) along 'h' [18].

2.4 Origin of Band Gap

The periodicity of electronic potential in semiconductors due to regular arrangement of atoms in a crystal lattice, results in the formation of forbidden energy bands for electrons (i.e.) the electronic band gap. Similarly the periodicity created in refractive index by artificially patterning a dielectric material to form a dielectric lattice of the PC results in the Photonic band gap. The band gap is a prominent factor that the control of radiation field and optical properties of the crystal depend upon. So we will look at the understanding of the physical origin of the band gap. Let us consider the simplest possible PC, which are alternate bi-layers of dielectric films. Consider light traveling entirely in the z-direction, crossing the sheets of dielectric at normal incidence. If the film is a uniform dielectric medium, with an artificially assigned periodicity 'a',

then we know that speed of the light is reduced by the index of refraction of the medium. So the frequency spectrum is just the light line [17] given by

$$\omega(k) = \frac{ck}{\sqrt{\varepsilon}} \qquad (2.1)$$

Where, c= speed of light in vacuum,

k= wave vector.

ε = dielectric permittivity.

Since k repeats itself outside the brillouin zone, the lines fold back into the zone, when they reach the band edges. As the refractive index contrast increases, the gap between these lines also increases. The gap occurs, at the edge of Brillouin zone, at k = (π/a). According to the electromagnetic variational theorem, the low frequency modes concentrate their energies in high ε regions, and low frequency modes, concentrate in high ε regions. So the band gap arises between these two at the edge of Brillouin zone. As the refractive index contrast increases, the band gap increases [17].

2.5 Electromagnetism in Photonic crystals

In order to study the propagation of light in a photonic crystal, we must turn to the Maxwell's equations. Maxwell's Equations governs the propagation of light through the PC.

The Maxwell's equations in C.G.S units are

$$\nabla \cdot B = 0$$

$$\nabla \cdot D = 4\pi\rho \qquad (2.2)$$

$$\nabla \times E + (1/c)\,(\partial B/\partial t) = 0$$

$$\nabla \times H - (1/c)\,(\partial D/\partial t) = (4\pi/c)\,J$$

Where E and H are electric and magnetic fields respectively, D and B are displacement and magnetic induction fields, and ρ and J are the free charges and currents respectively. *c* is a constant, speed of light in vacuum.

We need to deduce the general equation for the PC. We make some assumptions initially. The first assumption is that the medium has no free charges or currents, so set ρ= J=0.

The above equations become,

$$\nabla \cdot B = 0$$
$$\nabla \cdot D = 0$$
$$\nabla \times E + (1/c)\,(\partial B/\partial t) = 0 \qquad (2.3)$$
$$\nabla \times H - (1/c)\,(\partial D/\partial t) = 0$$

Second assumption is that the material is isotropic and we are in a linear regime. So that E(r, ω) and D(r, ω) are related by a scalar dielectric constant ε(r, ω). Ignoring explicit frequency dependence of dielectric constant, we have $D=\varepsilon E$.

The Maxwell's equations are further deduced to

$$\nabla \cdot B = 0$$
$$\nabla \cdot \varepsilon E = 0$$
$$\nabla \times E + (1/c)\,(\partial B/\partial t) = 0 \qquad (2.4)$$
$$\nabla \times H - (1/c)\,(\partial \varepsilon E/\partial t) = 0$$

Third assumption is that the dielectric constant is independent of frequency. We simply choose the value of dielectric constant appropriate to the frequency range of physical system we are considering. So $\varepsilon = \varepsilon(r)$. Then we restrict ourselves to only on low-loss dielectrics, so ε(r) is purely real. We know the quantities B and H are related by $B= \mu H$. Since for most of the dielectrics of interest magnetic permeability $\mu=1$, set B=H.

Now using all these assumptions we can deduce the final equation.

In general both E and H are complicated functions of time and space. But since the Maxwell's equations are linear, we can separate out the time dependence by expanding the fields into a set of harmonic modes. So we can write a harmonic mode as a certain field pattern times a complex exponential:

$$H(r, t) = H(r) \exp(i\omega t)$$
$$E(r, t) = E(r) \exp(i\omega t)$$

Inserting these in equation (2.4), the two divergence equations give us the conditions

$\nabla \cdot H(r) = \nabla \cdot D(r) = 0$.

The above equation means that there are no point sources and sinks of displacement and magnetic fields in the medium. Alternatively, the field configurations are built up of electromagnetic waves that are transverse.

The two curl equations relate to E(r) to H(r):

$$\nabla \times E(r) + (i\omega/c)\, H(r) = 0$$

$$\nabla \times H(r) - (i\omega/c)\, \varepsilon(r)\, E(r) = 0$$

Solving these equations for H(r), we get the master equation [17]

$$\nabla \times [(1/\varepsilon(r))\, \nabla \times H(r)] = (\omega/c)^2\, H(r) \qquad (2.5)$$

In addition to the divergence equation, $\nabla \cdot H(r) = \nabla \cdot D(r) = 0$, it completely determines H(r). The heart of Maxwell's equations for a harmonic mode in a mixed dielectric medium is a complicated differential equation for H(r), given the Master equation. The content of the equation is to perform a series of operations on a function H(r), and if that is an allowable electromagnetic mode, the result will just be constant times the original function H(r). This situation is called an eigen-value problem. If the result of an operation is just the function itself, multiplied by some constant, then the function is called an eigen function or eigen vector of that operator and the multiplicative constant is called the eigen value. We take $(\nabla \times ((1/\varepsilon(r))\ \nabla H(r))$ as a differential operator, that takes the curl, then divides by ε(r), and then takes curl again. For a given photonic crystal ε(r), we solve the master equation to find the modes H(r) for a given frequency, subject to transversality requirement. Then use the equation to recover E(r).

$$E(r) = -(ic/\omega\, \varepsilon(r))\ \nabla \times H(r).\ [17]$$

Solving this equation results in giving the eigen energy hω as a function of *k*, and is depicted in the Brillouin zone. The dispersion curve thus obtained is divided into the Photonic bands. The eigen state has a spatial pattern of E(r), and H(r) reflecting the symmetry of the lattice structure [17].

2.6 Photonic Crystals for Biosensing

The band structure of a given Photonic Crystal defines its optical properties, such as transmission and reflection. The refractive index contrast as we have seen earlier, is a very important aspect to get high band gap, and thus to have a good window to change the resonance wavelengths of the defects. Generally air is preferred as the low refractive index medium to have high contrast with the higher refractive index medium which is generally semiconductors which are selected depending on the

wavelength of interest. The fact that air is used as one of the mediums makes these artificial structures a very interesting choice to develop Bio sensors. The periodicity can be changed, to introduce both point and line defects. The effective periodicity can be changed by including an analyte and thus creating point defects, and the optical response of the analyte to various bio molecular events that take place within the defect and / or the whole lattice can be tuned in terms of the refractive index change. If we use a single defect, the intra band mode, produced by the defect is a localized mode. The surrounding crystal behaves as a mirror and thus the light is trapped in the defect, if we excite the crystal with wavelength of interest. The nano scale light matter interactions in the defects can be thus sensed and measured. The small scales of the lattice structure make the device very sensitive to changes in the defects. The localization effect which is very unique to photonic crystals, make these devices promising for bio sensor applications.

2.7. Biosensing Mechanisms

The bio sensing mechanisms using Photonic crystals are based on initiating various chemical mechanisms within a single lattice site (single defect) or a group of lattice sites (super defect) [7], or within the whole lattice structure, thus changing the refractive index and hence the optical properties of the crystal. The basic principle is that this change in refractive index can produce defects and thus localized states within the band gap, which are not present in the band gap otherwise. The refractive index is tuned and the localized state corresponding to that will also change. The band gap is a function of refractive index contrast of the substrate and interstitial material. So the substrate is selected to have a high refractive index, and based on the wavelength of interest. For exploring properties of photonic crystals at 1550nm wavelength, which is in the near infrared region, we have chosen silicon to be the substrate. Silicon has a refractive index of 3.46 at 1550nm. Similarly for visible wavelengths, we have chosen GaN (n=2.4). The interstitial medium spaces are filled with DI water (n=1.33) initially to have base results. The materials are chosen so that the refractive index contrast requirement is met. Also the materials are transparent at the given respective wavelengths. The two important parameters then are ‘a’ lattice constant, and ‘r’ the radius of each hole. These two are varied to optimize the band gap, given the

refractive index contrast. We can then change the refractive index of the interstitial medium, by some chemical means, or by introducing the analyte, which is to be sensed. The band gap variation can be measured as the refractive index of the interstitial medium changes.

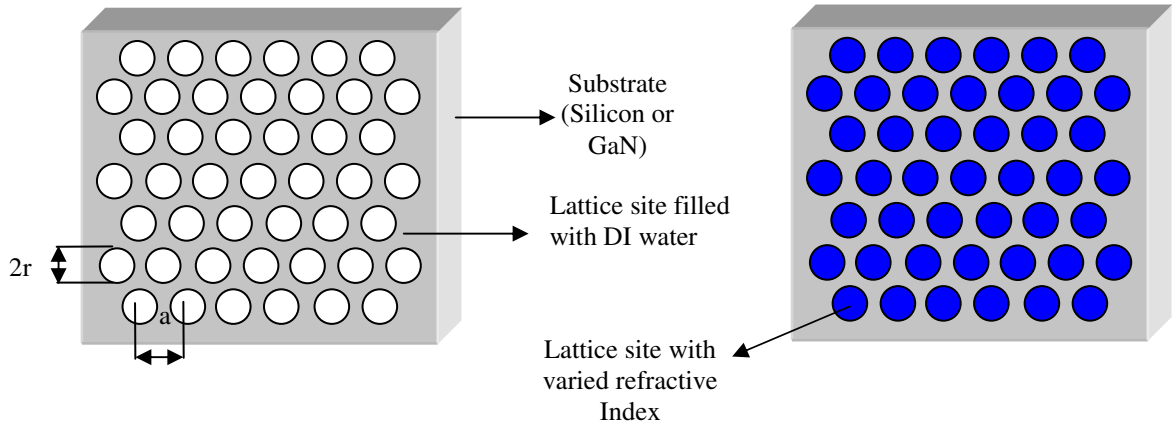

Figure 2.1: mechanism with refractive index change for the wh.ole lattice.

The second mechanism is forming a defect cavity targeting a single lattice site selectively. This is relatively more challenging than the above mechanism, given the dimensions of the lattice for the wavelength of interest. A defect cavity is formed by varying the refractive index of one lattice site and then the variations in the defect mode thus introduced in the band gap is measured in terms of the emitted wavelength.

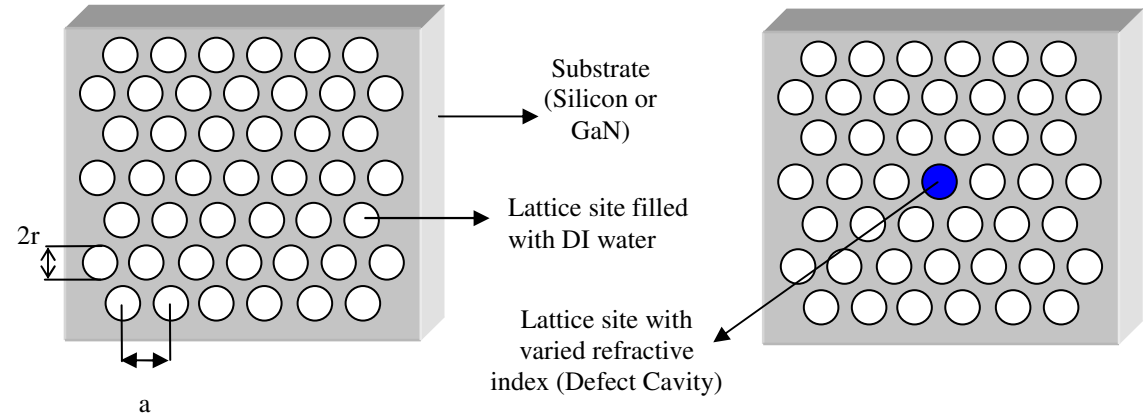

Figure 2.2: Mechanism with refractive index change for Single lattice site.

The next mechanism is similar to the second one. But instead of one lattice site, we can selectively target more lattice sites. The number of sites we target may vary from two to a whole unit cell (which is seven in the triangular lattice case). The change in emission wavelength of the number of lattice sites as a whole can be measured in terms of varying refractive index.

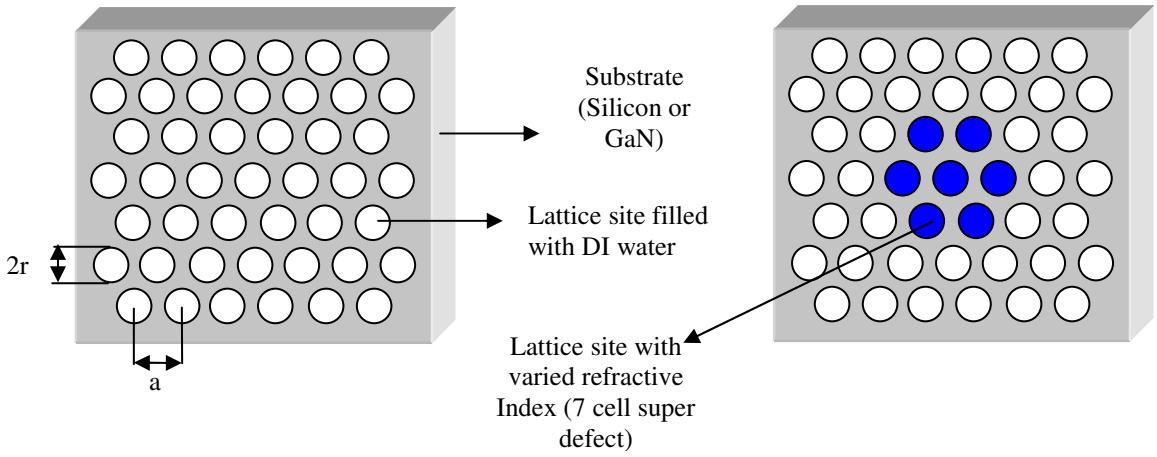

Figure 2.3: Mechanism with refractive index change for super lattice with 7 defects.

To compute the eigen states, and the localized modes, we need to solve the master equation (2.5), which requires complex a procedure. There are several tools which do this computation and give us the frequencies of the eigen states, and defect modes. Each tool uses different solution methods. This work uses the MIT photonics band package (MPB) [19], which is a frequency domain method, and FDTD, which is a time domain method from Optiwave [20]. We now familiarize ourselves with these two techniques.

CHAPTER III

DESIGN AND SIMULATION

3.1 Simulation and Modeling Techniques

Many methods for solving the master equation (equation 2.5) for the band structures have been proposed. All these methods fall in two broad categories, Frequency domain and time domain. There are advantages and disadvantages for each domain.

3.1.1. Frequency Domain

Frequency domain techniques do a direct computation of Maxwell's Equations to get the eigen states and eigen values. The master equation (2.5) is solved to obtain the allowed photon states, and their energies. Each eigen state has a definite frequency. These methods are used generally to calculate the band structures. This method iteratively solves the master equation and approximates the eigen states. The accuracy of eigen states increase as the number of iterations increases.

Advantages:

1. These methods directly provide the band structure.
2. Some modes might be closely spaced in frequency. These methods give those modes as separate eigen values in the result.
3. Since these methods iteratively solve for the eigen states, the error in the frequency in an eigen mode solver, decreases with more number of iterations.
4. The number of iterations doesn't change, even if we increase the resolution.

Disadvantages:

1. All of the lowest states up to the desired ones need to be computed, even if we don't want the lower ones.
2. These methods have poor convergence.

MIT Photonic Band package (MPB package) [19], which uses Plane Wave Expansion Method (PWEM), The Transfer Matrix Method (TMM) are some of the examples for Frequency domain techniques.

3.1.2. Time Domain

Time domain techniques iterate Maxwell's equations in time. These calculate the temporal evolution of the electromagnetic field propagating through the crystal. The band structure is then calculated using the Fourier transform of the field. These techniques are well suited to compute the evolution of field. These methods are generally used for finding resonant modes. This method is also used to calculate band structures. The Fourier transform is calculated and then the system's response for some input can be observed for peaks in the response. These peaks indicate the resonant modes.

Advantages:

1. The frequency spectrum which indicates the response of the system for various frequencies can be obtained at once from calculation based on a single field. Large frequency range can be obtained from one simulation.

Disadvantages:

1. Two states which are very close to each other in frequency might appear as a single frequency (single peak).
2. In Fourier transform, the frequency resolution is inversely proportional to the simulation time. So to get increased resolution in frequency, the simulation should be run longer.
3. To get good numerical stability, the time step for each simulation should be proportional to the spatial grid size, which depends on the wavelength. To get good spatial resolution, the simulation must be run for more number of time steps.
4. All the eigen states are not obtained at the same time with one simulation. For each eigen state, we need to run the whole simulation again.

Finite Difference Time Domain (FDTD) is a widely used time domain method.

We have used MPB package [19], to determine the dispersion relations and resonant frequencies and Optiwave FDTD method [1], to observe the wave propagation through the crystal.

3.2. Finite Difference Time Domain Method

Finite Difference Time domain (FDTD) is a simple technique in terms of implementation and also conceptually. FDTD as the name suggests is a time domain

technique to solve Maxwell's equations. It is based on solving the time-dependent Maxwell's curl equations, using Yee's algorithm [21]. The simplicity of the method lies in the fact that, if the 1-Dimensional implementation is understood, it is easily extended to 2, and 3- dimensional implementation. But as the dimension increases, the complexity of computation increases. This is because increase in the number of storage points, as the grid increases. Since the simulations here are limited to 2-dimensional, let us consider possible cases for 2-D simulation. The electric field perpendicular to the plane of propagation, which is the TE polarization and the magnetic field perpendicular to the plane of propagation, which is the TM polarization.

The Maxwell's equations are in linear isotropic regime are

$$\begin{aligned} \nabla \cdot B &= 0 \\ \nabla \cdot D &= 4\pi\rho \\ \nabla \times E + (1/c)\,(\partial B/\partial t) &= 0 \\ \nabla \times H - (1/c)\,(\partial D/\partial t) &= (4\pi/c)\,J \end{aligned} \qquad (3.1)$$

The third and fourth equations are the curl equations. Finite differences are introduced to these equations and then are solved.

$$B=\mu H$$

$$D=Ee$$

Considering these two equations, and assuming non conducting medium, we can set J=0, and assume ε, μ are constants.

The curl equations in 2-Dimensioanl becomes,

$$\begin{aligned} \frac{\partial}{\partial t}E_x &= \frac{1}{\varepsilon}\left(\frac{\partial}{\partial y}H_z - \frac{\partial}{\partial z}H_y\right) \\ \frac{\partial}{\partial t}E_y &= \frac{1}{\varepsilon}\left(\frac{\partial}{\partial z}H_x - \frac{\partial}{\partial x}H_z\right) \\ \frac{\partial}{\partial t}E_z &= \frac{1}{\varepsilon}\left(\frac{\partial}{\partial x}H_y - \frac{\partial}{\partial y}H_x\right) \end{aligned} \qquad (3.2)$$

$$\frac{\partial}{\partial t}H_x = -\frac{1}{\mu}\left(\frac{\partial}{\partial y}E_z - \frac{\partial}{\partial z}E_y\right)$$

$$\frac{\partial}{\partial t} H_y = -\frac{1}{\mu} \left(\frac{\partial}{\partial z} E_x - \frac{\partial}{\partial x} E_z \right)$$

$$\frac{\partial}{\partial t} H_z = -\frac{1}{\mu} \left(\frac{\partial}{\partial x} E_y - \frac{\partial}{\partial y} E_x \right)$$

These equations are similar to the equations (3.1).

The computational domain is a 2-Dimesional grid, with the pattern in the x-z plane. The 'y' direction is assumed to be infinitely large. The grid is as shown in figure.

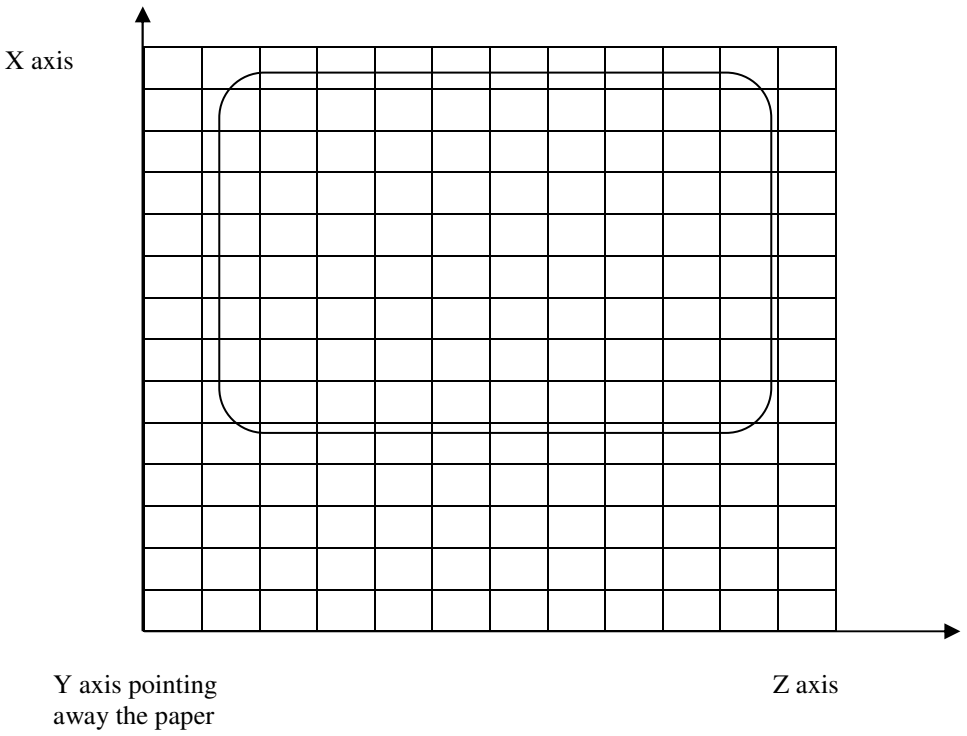

Figure 3.1: 2-Dimensional computational grid for solving the Maxwell's Equations using FDTD method [22]

We can now consider the polarizations, Transverse magnetic (TM), where Magnetic field is in a direction to the propagation direction and Transverse Electric (TE) polarization, where the electric field is perpendicular to the direction of the propagation.

For Transverse Electric Polarization

In the 2-D TE case, assuming 'z' as the propagation direction. So H_x, E_y, and H_z are non-zero components. The Maxwell's equations becomes

$$\frac{\partial}{\partial t}E_y = \frac{1}{\varepsilon}\left(\frac{\partial}{\partial z}H_x - \frac{\partial}{\partial x}H_z\right)$$

$$\frac{\partial}{\partial t}H_x = \frac{1}{\mu}\left(\frac{\partial}{\partial z}E_y\right) \qquad (3.3)$$

$$\frac{\partial}{\partial t}H_z = -\frac{1}{\mu}\left(\frac{\partial}{\partial x}E_y\right)$$

Each filed is represented by a 2-D array, $E_y(i,k)$, $H_x(i,k)$, $H_z(i,k)$, where i, k are indices for time steps along 'x' and 'z' directions.

Localization of TE fields in the grid is shown in figure 3.2.

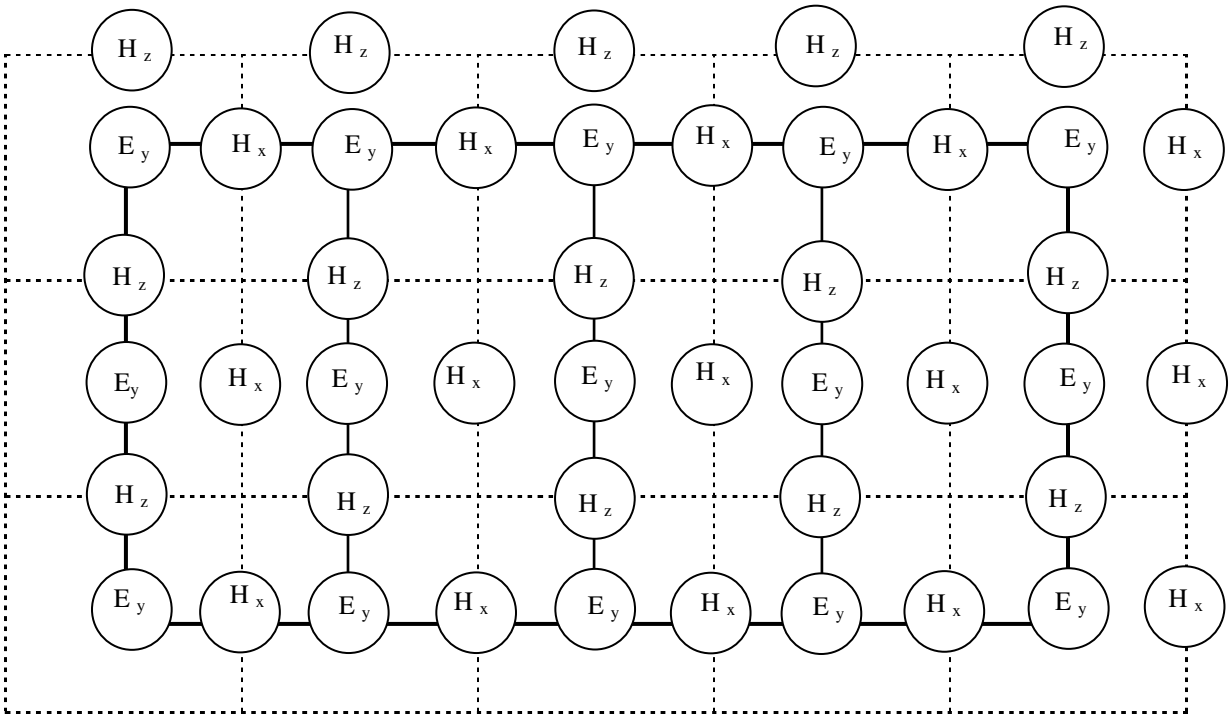

Figure 3.2: Position of fields in computational domain [22].

The domain is divided into many FDTD space cells, with each cell having specific positions for different fields, in terms of (i, j). The E_y field is the center of the FDTD space cell. The H_x and H_z fields are ate a position at increment of 0.5 in respective direction. So if the E_y field is at indices (i, j), then the indices for H_x is (i , k+0.5), and for H_z it is (k, i+0.5). Also each node in the mesh is associated with information about the

refractive index at that point. So the fields at each node are calculated, for a given set of time steps, as the light propagates through the crystal. This ordering is repeated throughout the grid. [22]

Central differences are applied to the equations (3.3), and the resulting equations are:

$$\frac{E_y^{\,n}(i,k) - E_y^{\,n-1}(i,k)}{\Delta t} =$$

$$\frac{1}{\varepsilon}\frac{H_x^{\,n-1/2}(i,k+1/2) - H_x^{\,n-1/2}(i,k-1/2)}{\Delta z} - \frac{1}{\varepsilon}\frac{H_z^{\,n-1/2}(i+1/2,k) - H_z^{\,n-1/2}(i-1/2,k)}{\Delta z}$$

This equation can be rewritten as

$$E_y^{\,n(i,k)} = E_y^{\,n-1}(i,k) +$$

$$\frac{\Delta t}{\varepsilon \Delta z}\left[H_x^{\,n-1/2}(i,k+1/2) - H_x^{\,n-1/2}(i,k-1/2)\right] - \frac{\Delta t}{\varepsilon \Delta z}\left[H_x^{\,n-1/2}(i+1/2,k) - H_x^{\,n-1/2}(i-1/2,k)\right]$$

$$H_x^{\,n+1/2}(i,k+1/2) = H_x^{\,n-1/2}(i,k+1/2) + \frac{\Delta t}{\mu \Delta z}\left[E_y^{\,n}(i,k+1) - E_y^{\,n}(i,k)\right] \qquad (3.4)\ [22]$$

$$H_z^{\,n+1/2}(i+1/2,k) = H_z^{\,n-1/2}(i+1/2,k) - \frac{\Delta t}{\mu \Delta x}\left[E_y^{\,n}(i+1,k) - E_y^{\,n}(i,k)\right]$$

'n' indicates the time step, and I, k labels the space steps, along x and z directions.

Similarly the equations for a TM polarized wave are

$$\begin{aligned}
\frac{\partial}{\partial t}H_y &= \frac{1}{\mu}\left(\frac{\partial}{\partial z}E_x - \frac{\partial}{\partial x}E_z\right) \\
\frac{\partial}{\partial t}E_x &= -\frac{1}{\varepsilon}\left(\frac{\partial}{\partial z}H_y\right) \qquad (3.5) \\
\frac{\partial}{\partial t}E_z &= \frac{1}{\varepsilon}\left(\frac{\partial}{\partial x}H_y\right)
\end{aligned}$$

The computational domain is same as that for the TE case. But the H_y field is located at the center of space cell and E_x, and E_z are at the cell edges. The algorithm for the numerical discretization is similar to that of TE case.

The selection of grid size and the number of time steps is very important for this method. The space grid is chosen such that the electromagnetic field doesn't change considerably [21]. This implies that the space step is approximately fraction of wave length. The time step is determined to have numerical stability of the algorithm. We chose $\Delta x = \Delta y = \Delta z$. For a constant ε and μ, the stability requires that [21, 22].

$$\Delta t \leq \frac{1}{c\sqrt{\frac{1}{(\Delta x)^2} + \frac{1}{(\Delta y)^2}}} \quad ,$$

Where 'c' is the velocity of light in air. But if c_{max} is the max wavelength in the region, then the stability criterion becomes [22]

$$\Delta t \leq \frac{1}{c_{max}\sqrt{\frac{1}{(\Delta x)^2} + \frac{1}{(\Delta y)^2}}} .$$

The flow chart for the simulation process is as shown in figure 3.3.

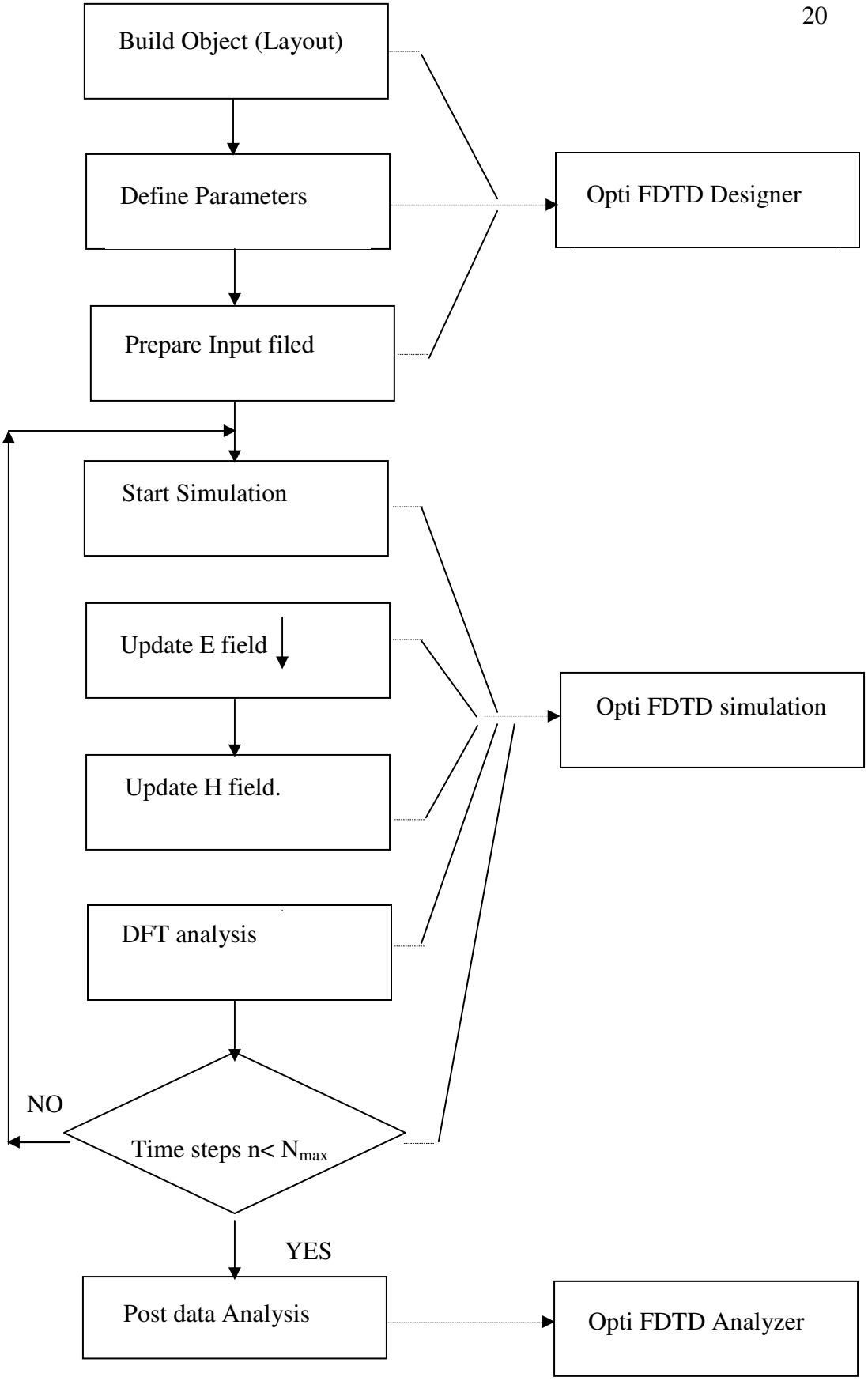

Figure 3.3. Flow chart for simulation process [22].

3.3. Simulation Results

3.3.1. Introduction

Photonic crystals are classified as 1-D, 2-D and 3-D photonic crystals depending on the directions in which they offer periodic variation of refractive index. There are different geometries and structures. The structure which contains air holes in a dielectric is most suitable for developing biosensors because the air holes can be effectively used to fill with the analyte of interest and thus create defects. The selection of a structure depends on the application. The 1-D Photonic crystal is the fundamental type Photonic crystal. It consists of alternate layers of dielectric materials. Bragg reflector is an example of 1-D photonic crystal. The propagation is along only one direction. The band diagrams can be easily anticipated considering them as Bragg reflectors. The 2-D photonic crystals contain the periodic variation of refractive index in 2 dimensions. There are two main directions in which the propagation is to be considered. 3-D photonic crystals offer variation of refractive index in all the three directions. These structures offer complete photonic band gaps, which means light can be modulated in all three directions for all angles of incidences and for all polarizations. But these are very difficult to achieve. 2-D Photonic crystal slabs with 2-D geometry and with a specific thickness in the third dimension can be used to obtain complete band gap. The mechanism of guiding is through total internal reflection along one direction (perpendicular to the direction of the plane containing photonic crystal), and through photonic crystal diffraction along the 2 dimensions containing the crystal lattice. These are relatively easier to fabricate than 3-D photonic crystals. The two basic structures are square and triangular. Square structures contain holes in dielectric in a square lattice. The triangular lattice structure contains air holes in a hexagonal symmetry. The brillouin zone of triangular lattice is close to a circle. This structure exhibits higher symmetry than the square structure. This lattice is selected for its higher symmetry, which gives us overlap of TE and TM band gaps. Let us consider the band gap and dispersion relation for the triangular lattice.

3.3.2. Design of Parameters

The triangular lattice is shown in figure 3.4.

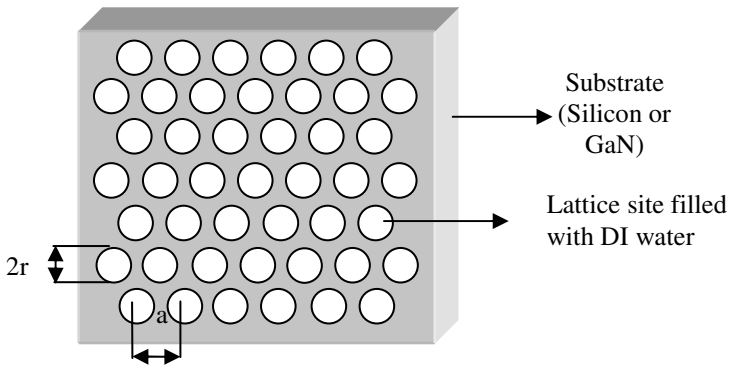

Figure 3.4. Triangular lattice structure

After the structure was chosen, the materials best suited for the application, and parameters 'a', and 'r' were to be chosen. The first parameter to be selected is the refractive index of the materials. We should choose the material so that it has a high refractive index contrast with the material filling the interstitial medium. The higher the refractive index contrast between these two media, the higher is the band gap. The devices of interest are to be operated at 1550nm and at 550nm. The materials chosen are therefore silicon for 1550nm and GaN for 550nm. These materials have high refractive indices at the wavelengths of interest. The interstitial medium was considered to be DI water for simulation purposes. The refractive index value for silicon is assumed as 3.46, and for GaN it is 2.4 at the wavelengths of interest. The refractive index value of DI water is assumed to be 1.33. Any design of a photonic crystal lattice depends on the dispersion relations. The choice of 'a', and 'r', is important to determine the dispersion relation. The dispersion relation gives the allowable frequencies, and the band gap in terms of normalized frequencies. Also the 'r' is chosen as a normalized value in terms of 'a'. We have to choose a value of 'r', so that the band gap is a maximum. Then for a given (r/a), we can have the dispersion relations in terms of normalized frequencies. Since Maxwell's equations are scalable, from the normalized frequencies we can scale the parameters to the wavelength of our interest.

3.3.2.1. (r/a) Vs Band gap

The Band gap is dependent on many factors, as we discussed earlier. For a specific structure given the lattice structure, we have different band gaps for different (r/a). Figures 3.5 and 3.6 give us the variation of percentage gap, which is the measure of band gap, with varying (r/a). The band gaps in the figure were TE (Magnetic field perpendicular to the plane of propagation) band gaps. These results were obtained from MPB package [19].

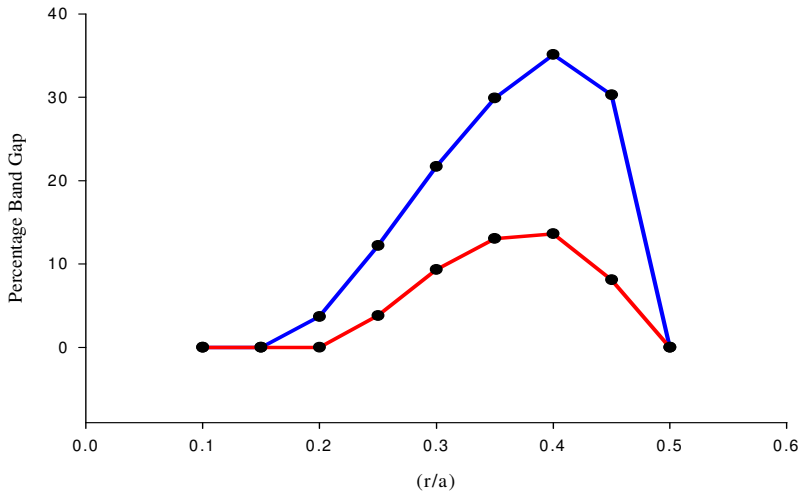

Figure 3.5. Variation of percentage band gap with different (r/a) for triangular lattice of holes in dielectric

Silicon (n=3.46), Vs DI water (n=1.33)

GaN (n=2.4) Vs DI water (n=.133)

The percentage band gap is the ratio of the difference in the normalized frequency values of the band edges to the mid band normalized frequency [19].

$$\%\ \text{band gap} = \frac{Upperbandnormalizedfreqency - Lowerbandnormalizedfrequency}{MidbandgapNormalizedfrequency}$$

The band gap for both refractive index contrasts silicon vs DI water and GaN vs DI water, is highest at the normalized radius value (r/a) =0.4. As a result, the dispersion relations at this value of (r/a) were explored.

3.3.2.2. Band Diagrams

The band diagrams are computed by solving the master equation (2.5). For each value of 'k' (wave vector), the equation results a set of modes whose frequencies vary as function of k. All these modes are allowable modes which propagate through the crystal. We get continuous curves of ω_n (k). Also we get for each k different set of curves. These curves give the information about the modes in the crystal. These curves which are distributed along different frequencies are the dispersion relation, which are also called the band diagrams. Band diagrams give all allowable modes, and the band gap, where there are no allowable modes for specific symmetry of the crystal. These band diagrams vary depending on the 'a' (lattice parameter), 'r' (radius of each hole), and also the polarization of the input wave. The band gap variations with 'r', and polarization were explored for the hexagonal lattice. The simulation procedure is explained in Appendix A.

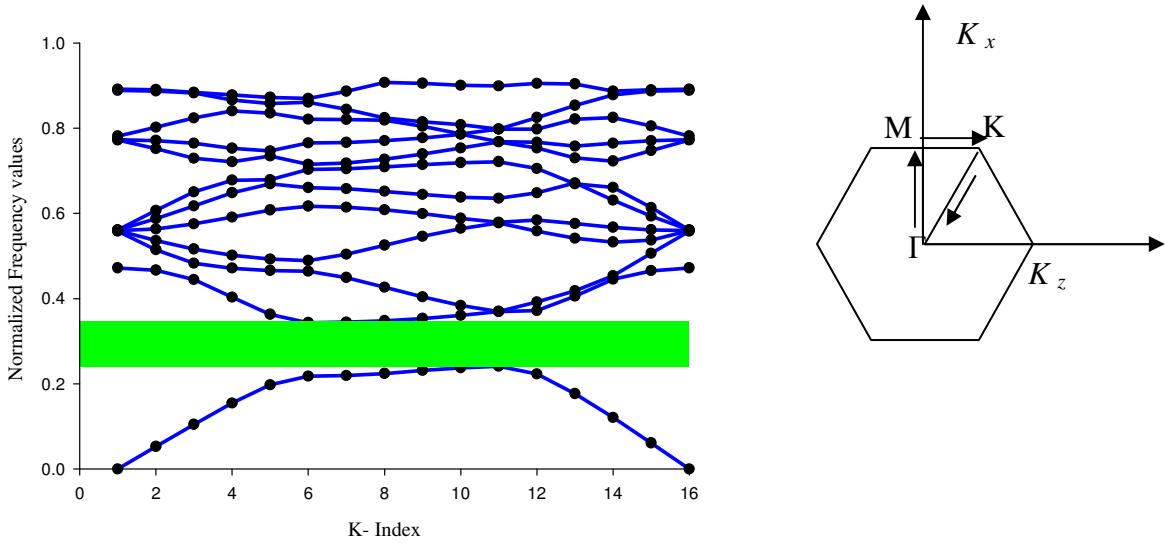

Figure 3.6. Dispersion relation (band diagram) for triangular array of holes, (r/a) =0.4, and Silicon(3.46) Vs DI water (n=1.33). The Brillouin zone is also shown.

Figure 3.6 is the dispersion relation for the triangular lattice shown in figure 3.4. The (r/a) is 0.4, and the dispersion relation is for TE band gap for silicon and DI water. The *k* index is the *k* - path from Γ to M to K and then back to Γ, in the brillouin zone shown in the figure 3.6. Each path is divided into 4 divisions. The band gap range is 0.2409 to 0.3479 (normalized frequency scale).

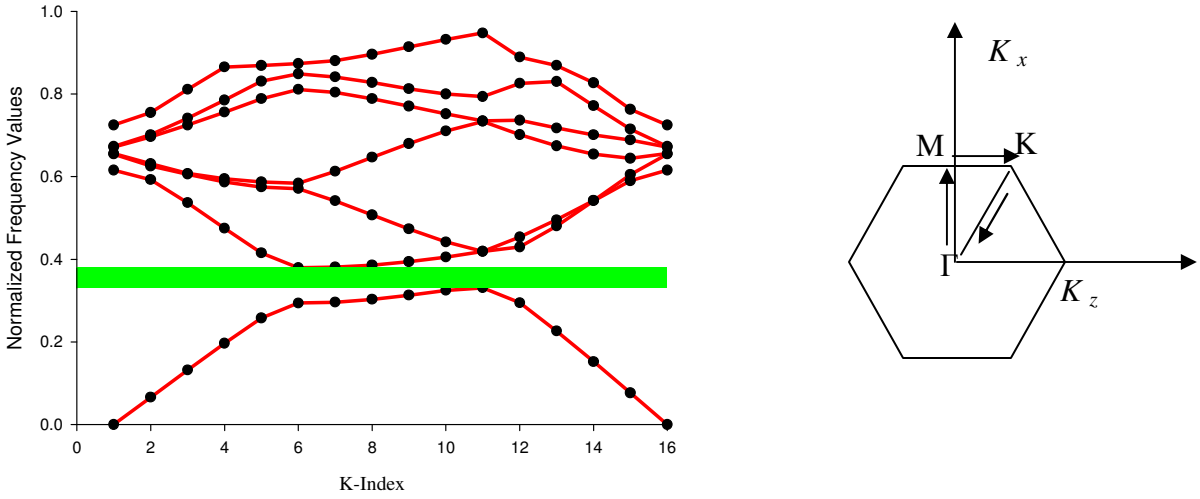

Figure 3.7. Dispersion relation (band diagram) for triangular array of holes, (r/a) =0.4, and GaN (2.4) Vs DI water (n=1.33). The Brillouin zone is also shown.

Figure 3.7 is the dispersion relation of a triangular array of holes, with (r/a) =0.4 for GaN (n = 2.4), vs DI water (n=1.33). The band diagram is for TE polarization. The band gap is from 0.3308 to 0.3792 in the normalized frequency scale. The selection of 'a' and 'r' depends on the wavelength of interest. For silicon, the wavelength of interest is 1550nm. So the normalized frequency of the defect is scaled to 1550nm.

$(a/\lambda)_{Norm}$ = Normalized frequency value of the defect. We want the wavelength at 1550nm. So we can get the value for 'a', and then we can determine the 'r' value. For this case, the (r/a) used was 0.4. A similar process was adapted for the GaN case as well in order to design the values of 'a' and 'r'.

3.3.2.3. Defect States

The dispersion relation gives information about all allowable and non allowable modes that propagate through the given triangular array of the hole structure. Defect states within the band gap can be created by introducing defects in the crystal. Defects can be introduced by changing the size, shape, and/or refractive index of one of the lattice sites (point defects) or a line of lattice sites (line defects create a wave guide defect.). The introduction of defects in the lattice introduces modes in the band gap which are not allowed to propagate in the perfect crystal. The wavelength of the defect modes depend

on the defect introduced, and changes with the change in properties of the defect. The optical properties of the photonic crystal are very sensitive to the changes in defects. Simulations corresponding to defects created by changing the refractive index of one or more lattice sites were completed. The change in emission wavelength of the defect with change in refractive index of the defect was explored.

The defect wavelength change for change in refractive index from 1.33 to 1.34 in steps of 0.001 is given in figure 3.8

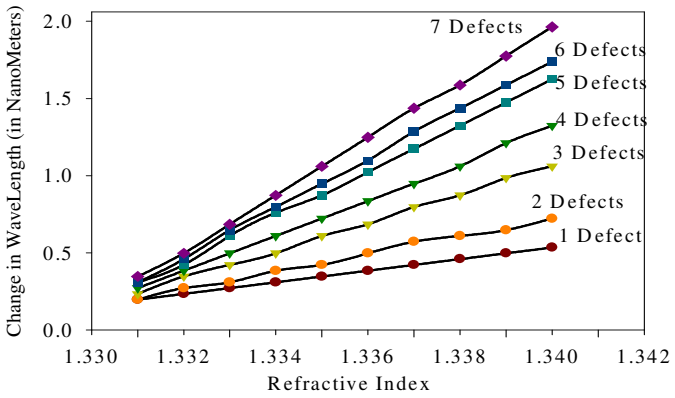

Figure 3.8. Change of wavelength Vs Change of refractive index for 1 to 7 defects in unit cell.

The refractive index of the defect is varied from 1.330 to 1.340 in steps of 0.002, and the resulting change in emission wavelengths was plotted. The change from 1.33 to 1.53 in steps of 0.02 is also plotted for both the cases (refractive index contrast of 3.46 Vs 1.33 and 2.4 Vs 1.33).

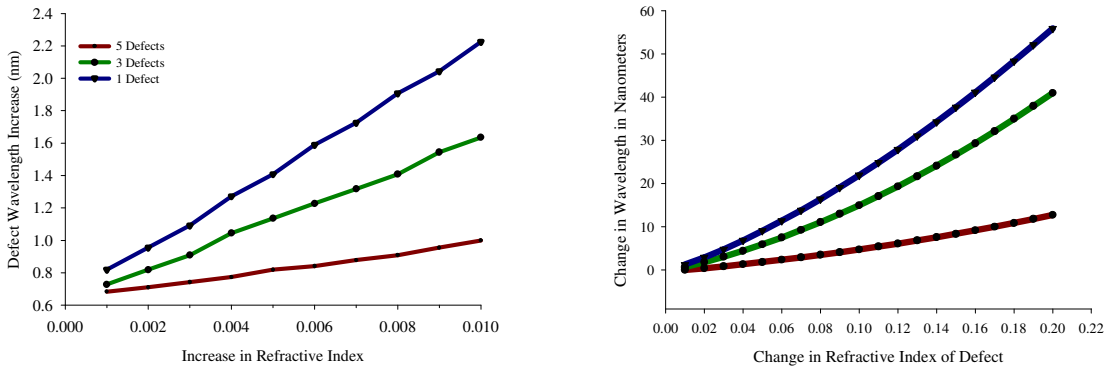

Figure 3.9. Change of wavelength Vs Change of refractive index for silicon Vs DI water for 1, 3, and 5 defects. Both fine and coarse changes were plotted.

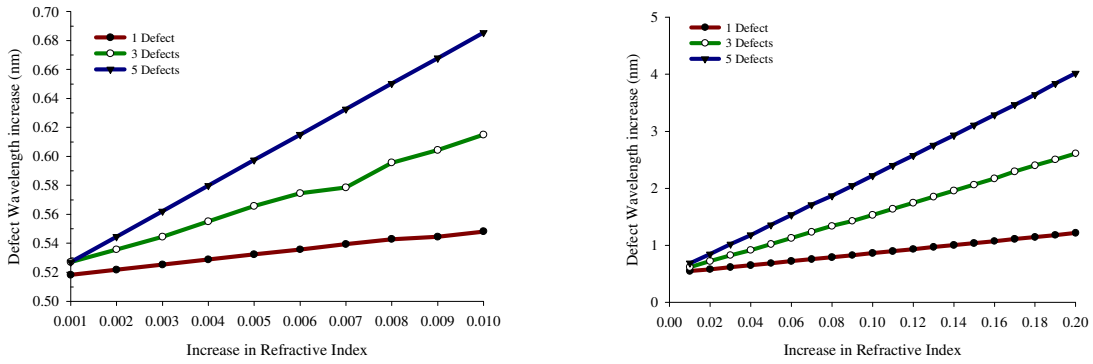

Figure 3.10. Change of wavelength Vs Change of refractive index for GaN Vs DI water for 1, 3, and 5 defects. Both fine and coarse changes were plotted.

The emission wavelength change is increasing with the number of defects. The wavelength changes can be detected for change in refractive index values as low as 0.001. With suitable detectors the change in wavelength with small changes in wavelength can be detected. The pattern features were several hundreds of nanometers for silicon and tens of nanometers for GaN. The fabrication of these small features is very challenging. The efforts to fabricate prototype PCs in silicon will be discussed in the next chapter.

CHAPTER IV
FABRICATION

4.1. Introduction

With the simulation results and design parameters available our focus now turns to the challenging aspect of PC fabrication. As the design and simulation results indicate, the design parameters like, lattice constant ‘a’, the radius of each hole, ‘r’ are on order of hundreds of nanometers. Also even a few nanometers change in the patterns can change the optical properties of the crystal. So it is very crucial to obtain the patterns with very high precision both in size and shape. In addition to the small size of the PC lattice, the precision required for fabricating these patterns makes the fabrication part even more challenging. Different methods can be used to fabricate the photonic crystals. There are different procedures for fabrication, which vary depending on materials of interest, equipment used, and mask used for transfer of patterns [23, 24]. E-Beam Lithography is typically the best method to fabricate 2-D photonic crystals with the unit cell patterns sizes of interest. This chapter explains the fabrication protocol developed as a part of this work for fabricating 2-D photonic crystals using e-beam lithography and presents the analysis of results obtained.

4.2. Fabrication Methods

There are different methods of fabricating 2-D photonic crystals. First successful Photonic crystal was created by drilling holes into ceramic material, which is now called Yablonovite [25]. The structure created was an array of holes with diameter of six millimeters, and it effectively blocked radio waves from 13-16 Giga Hertz [25]. The fabrication of photonic crystals for infrared and the visible light wavelength region require lattice elements of sub micron range. Much more sophisticated processes are required for fabrication of these structures. The rapid progress in lithography techniques, and invention of sophisticated equipment for these lithographic processes, made the fabrication of these sub-micron structures easier though still challenging to fabricate. Optical lithography can be used to accomplish the task. But this method has some limitations. Resolution of the patterns may not be as desired because of the wavelength of

source. The sub micrometer patterns are difficult to achieve using optical lithography. Better sources of very short optical wavelengths are needed to obtain the patterns which are of a few hundreds of nanometers. The literature reports lithography being used at deep UV wavelengths with excimer lasers with wavelengths starting at 248nm and 193nm and research conducted at 153nm [26, 27]. However the usage of optical lithography imposes a limitation on the size of the patterns. E-beam lithography is a very effective method to control the fabrication of these small patterns. E-Beam lithography is best suited for fabrication of these nanometer patterns. In E-Beam lithography an electron beam is focused and the patterns are written on the resist. The main limitation of this process is the slowness of the writing. However this method is the most used technique for research purposes. The resolution obtained using these methods are best suitable for the PC patterns of our interest.

4.3. Fabrication Procedure

The basic recipe for fabrication of 2-D photonic crystals is as shown in the figure 4.1. E-Beam lithography was used to write the patterns on a positive resist. The pattern is obtained by developing the resist. Then the pattern is then transferred onto silicon by dry etching.

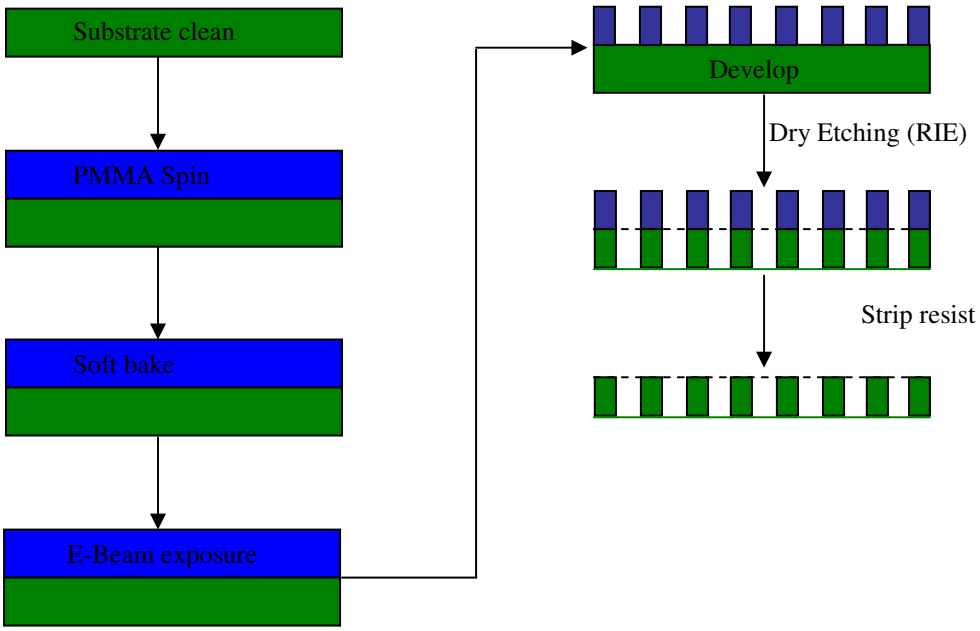

Figure 4.1. Process steps for fabrication of 2-D photonic crystals.

4.3.1. Process Steps for Fabrication

Step 1: Sample clean:

The substrate used here was silicon. The silicon sample was cleaved using a diamond scribe. The sample size should be around 2cms x 2cms, to fit the on the sample holder in the E-Beam system. An organic clean was done by soaking the sample in Acetone for 5 minutes and then in Methanol for 5 minutes. Substrate is dried using Nitrogen gas.

Step 2: Resist spin

PMMA is a positive resist, which is used for E-Beam lithography [28]. In this process PMMA is used as a mask to transfer patterns on silicon. PMMA is a high contrast, high resolution resist for Electron beam which is used to get very small patterns. PMMA is most common resist used for E-Beam lithography. PMMA is the synthetic polymer of Methylmethaacrylate. The carbon - carbon double bond in CH2=C(CH3)COOCH3 naturally polymerizes to form PMMA. On exposure to E-beam, the long chains of PMMA break (scission), and are easily soluble in developer.

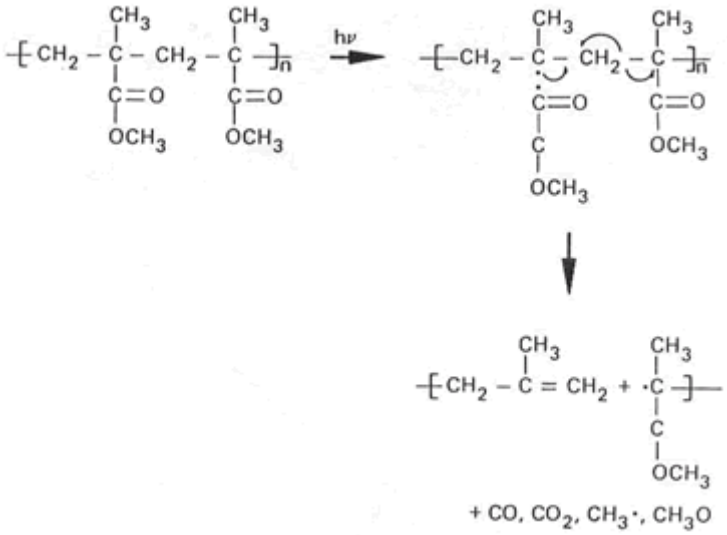

Figure 4.2. Polymer breaking by exposure to Electron beam [29].

There are different types of PMMA. The PMMA is chosen depending on the thickness of resist required. The research started with PMMA 495 A2 [28] (PMMA of molecular weight 495 2% in Anisole). Using PMMA 495 A2, we can spin resist layer as

thin as 80 nm, at a speed of 4000rpm, from spin speed curve shown in figure 4.3. But the patterns were to be patterned on a thin slab waveguide which supports a single mode. To obtain this we need a thicker resist. So the next set of E-beam exposures was done on a thicker layer of resist, PMMA 950 A4 (PMMA of molecular weight 950 4% in Anisole). The thinnest layer that can be spun using this PMMA is 200nm at 4000 rpm, from the spin speed curve in figure 4.4. The spin programs are given in Appendix B. The resist is spun on the silicon sample and then baked on hot plate at a Temperature of 180 degrees for 75 seconds [28].

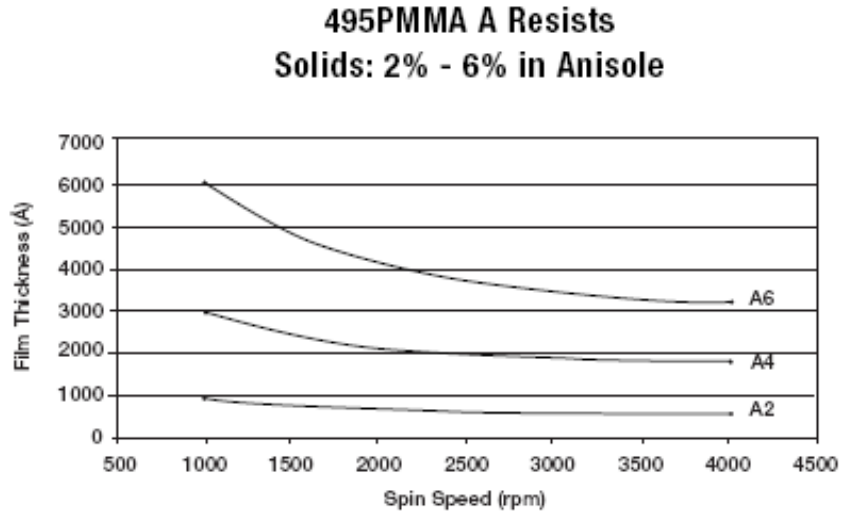

Figure 4.3. Spin-Speed curve for PMMA 495 A2 resist [28].

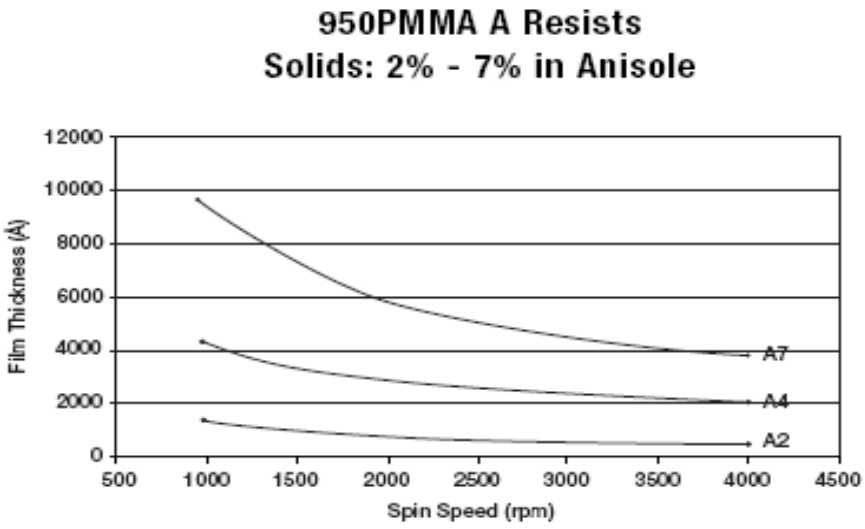

Figure 4.4. Spin-Speed curve for PMMA 950 A4 resist [28].

Step3: Electron beam Lithography

Electron Beam Lithography (EBL) is a non optical lithography technique where an electron beam is used to write the patterns. Direct write E-beam lithography takes more time than optical lithography. But when smaller features are required with very high resolution, this is a very effective method. Generally an electron sensitive resist is used as a mask to transfer the patterns on to substrate. The resists used undergo certain chemical changes when exposed to the electron beam. The resists may be positive or negative, depending on how they change on E beam exposure. For positive resists, the exposed regions become more soluble, and thus when developed are removed. Where as for negative resists, the exposed regions become less soluble, and thus when developed the unexposed regions are removed. The advantage of positive resist is that after development the pattern remained can be used exactly as a mask. For negative resist, the remaining patterns after development are the reverse of mask patterns. PMMA is a positive resist. In E-beam lithography, the electrons interact with, atoms in the surface. Electrons can go undeflected, or scatter elastically or inelastically. The electron beam energy defines the penetration depth. General Optics scheme for E beam lithography is as shown in figure 4.5. A typical E-beam lithography system consists of electron gun, which is the source for electron beam, lenses and apertures, to focus the beam, mechanism for deflecting the beam, beam blanker, stigmator, and electron detectors [30] . The E-beam lithography system we used was Leica Cambridge SEM Stereoscan S360. This E-Beam lithography system is enabled with NPGS software [31]. NPGS software has the capability of importing many file formats. The pattern can be designed using design softwares like L-EDIT and Design CAD LT 2000. Design CAD LT 2000 was used to design patterns with .dc extension. These files are converted into *ASCII.DC2* format by NPGS software. The format of the writing can be selected in such a way that the beam in a single pass writes the pattern top to bottom in a zigzag fashion. The design of patterns using Design CAD LT 2000 software is given in the Appendix A.

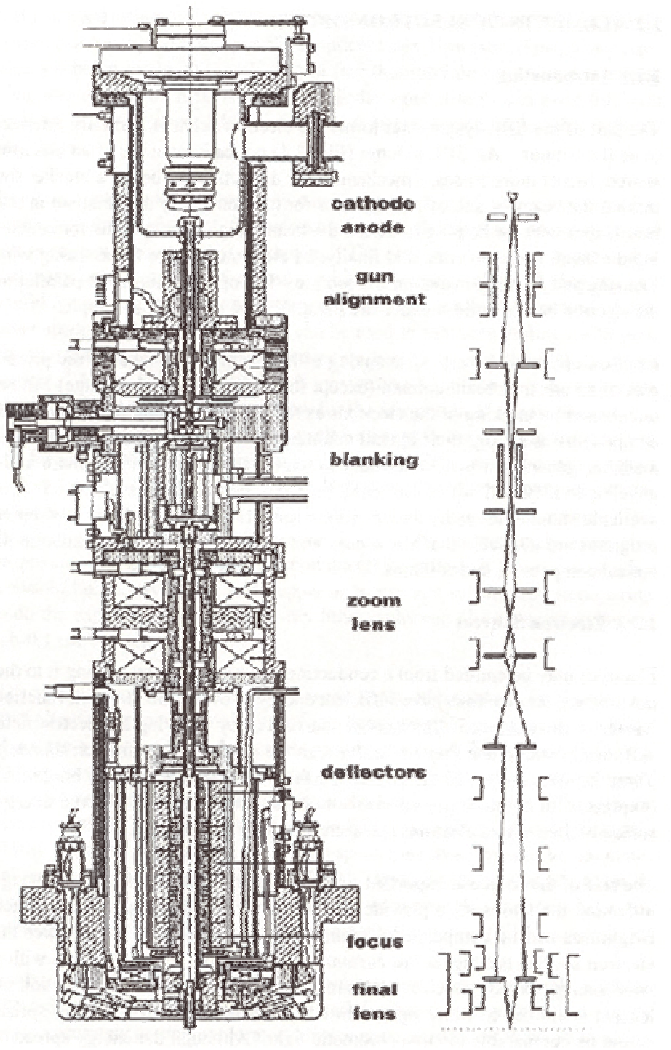

Figure 4.5. General optics scheme for E Beam Lithography [30]

The design file is converted into run file (*.rf6* extension), with the write parameters such as Probe Current, Magnification, and Dose set to required values. Before writing the pattern, the filament current is adjusted such that the beam spot is circular, and this spot should be adjusted to be at the center on the screen. We should make sure that Beam blanker is ON. The voltage for beam blanker is set to a value such that no emission is seen, and the beam is moved of the sample when it is ON. Then the beam voltage is increased to desired value. The brightness, contrast and focus are adjusted. The probe current is set to desired value. The magnification in SEM is changed to the value of magnification required to write the pattern. The mode is changed to NPGS (*write* mode)

and then the write file (*.rf6* extension file) is processed by clicking process run file option.

Specifications:

- Acceleration Voltage: 0.2-40KV
- Resolution: Tungsten (W) cathode -5nm.
- Magnification: 5-300K
- Detector: Secondary electron detector, back scattered electron detector
- Specimen chamber: 270X 270X 250mm
- Stage: computer controlled motorized, movements X/Y=100m, Z=70mm, tilt angle =90^{o}, rotation=360^{o}.
- Accessories: High resolution display, optical and Winchester disk image storage systems, viewing window and digital capture and image transfer.

Step 4: Develop PMMA

PMMA, being a positive resist, the areas where it was exposed to electron beam, become more soluble than the other areas. The exposed patterns should be removed. The removal process is a two step process. The resist is developed in MIBK (Methyl Isobutyl Ketone): IPA (Iso propanal Alcohol) 1:1 for 30 seconds and then in 1:3. The first step is a faster developing process and the second step slows the development. The areas exposed to the E beam are removed and this creates the pattern in PMMA. To develop the patterns in silicon, this pattern in PMMA is used as a mask. The patterns are transferred by using Reactive Ion Etching (RIE).

Sputtering:

During the process, the patterns on PMMA are to be optimized to get the desired sizes. The samples are viewed in SEM. The sample is coated by a thin layer of metal, to ensure that the charging of resist is prevented. Charging of resist may cause unwanted distortion of the pattern. The thin layer of metal is sputtered CVC 610 sputtering deposition system. Platinum was sputtered on the samples because of its small grain size. The thickness of metal deposited was about 40nm. The sputtering process and specifications for the process are explained in Appendix B.

A simple sputtering system is a D.C. magnetron reactor operated under vacuum. In sputtering atoms from target are physically removed. Inert gas such as Argon (Ar) is used to create high density of ions, and these ions bombard the target. These ions break the bonds between atoms and the solid, and the atoms are physically removed. The sample is placed on anode, and the target on cathode. The sputtered atoms are thus deposited on to the sample.

4.4. FABRICATION RESULTS

4.4.1. Direct Write on PMMA 495 A2

The sample holder stage in E-beam lithography system is as shown in the figure 4.6.

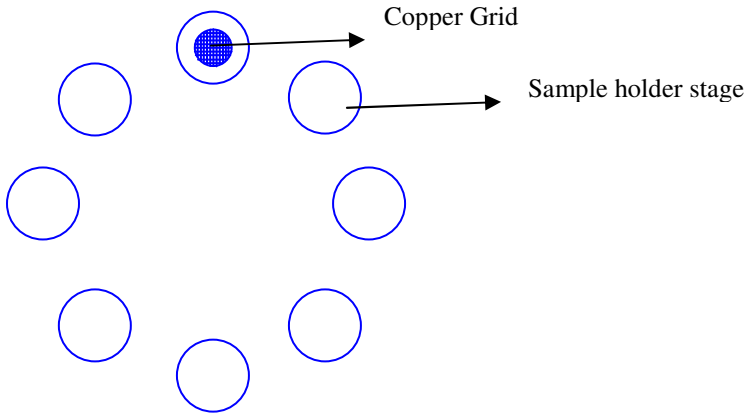

Figure 4.6 Sample holder stage

The stage contains 7 sample holders, and one holder containing the copper grid. Before writing, the copper grid is mad sure to be under the beam. The stage has specific X, Y, and rotation. Once the X, and Y distances are set so that the copper grid is right at the center of the screen, which means that copper grid is exposed to the beam first. The focus, at required EHT voltage, and at required magnification are set first on the copper grid, and them the stage is rotated till we see sample edge. The focus is then set on the sample. The beam blanker is switched ON. The distances between centers of the sample holders were previously determined [32], as 1.25 (in the rotation). The mode is now changed to NPGS and them writing is done. The sample is kept on the sample holder, and

the exposure dose is varied, since exposure dose is found to be better metric than dwell time [32]. The first pattern tried was ‘star’ pattern, which is shown in the figure 4.7.

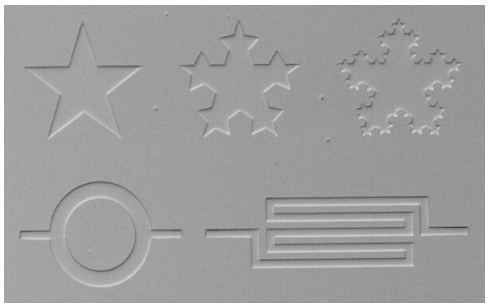

Figure 4.7. Star pattern.

The writing started with PMMA 495 A4. The patterns designed were a triangular array of holes, designed by Design CAD LT-2000 software. The design procedure was explained in Appendix A. The resist was 80nm thick. After writing the patterns, the sample was sputtered with 40 nm thick Platinum and the sample was viewed under the SEM. The patterns were first done with spin program 1 shown in Appendix B.

Conditions for the writing of the pattern.
EHT voltage =30KV
Filament current =2.5 A (first peak)
Probe current =49.9pA.

Table 4.1 Pattern position on sample1

X-Position ↓ →Y-Position	575	580	585
330	a*		
335	B	C	D
340	G	F	e*
345	H	I	

*-star patterns

Table 4.2 Doses for patterns with 'a'=2 microns, and 'r'= 800nm on sample 1.

Pattern	Magnification	Dose (in μC/cm^2)	Time (in Seconds)
A	647		
B	2.69k	50(by mistake this was given as line dose)	13.4minutes
C	2.69k	50	4.1
D	2.69k	100	8.1
E	647		39.4
F	2.69k	100	8.1
G	2.69k	150	12.1
H	2.69k	200	16.1
I	2.69k	250	20.1

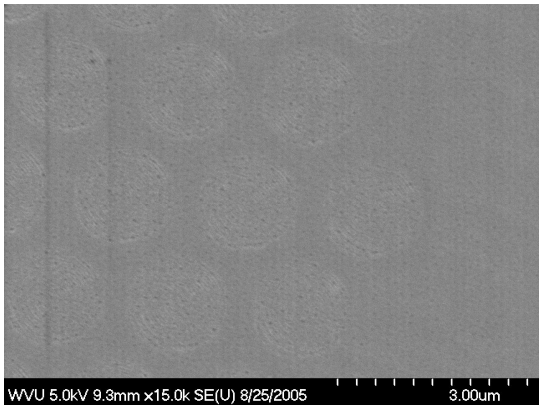

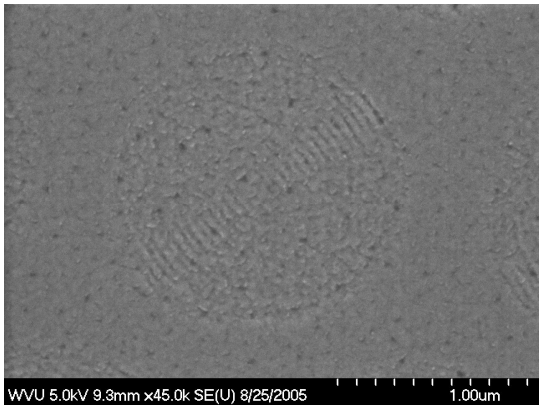

Figure 4.8. SEM images Pattern 'g', Dose 150 μC/cm^2(resist thickness 80nm)

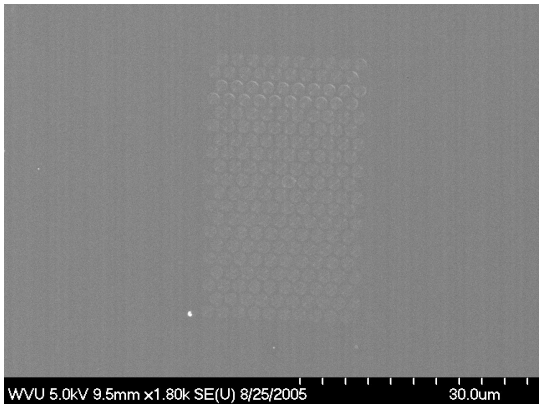

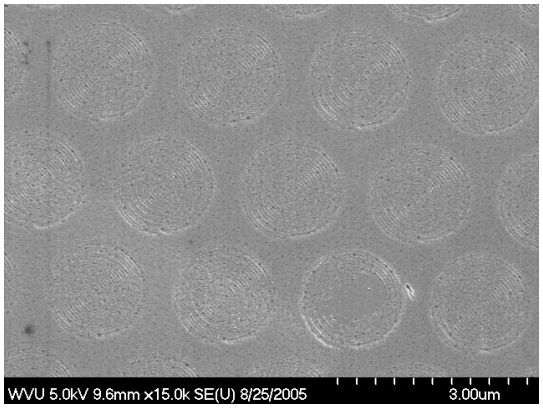

Figure 4.9 SEM images of Pattern 'h', Dose200 μC/cm^2(resist thickness 80nm)

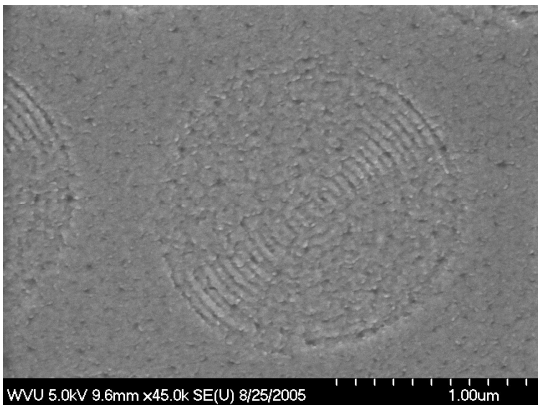

Figure 4.10 SEM image of Pattern 'h', Dose200 μC/cm^2(resist thickness 80nm)

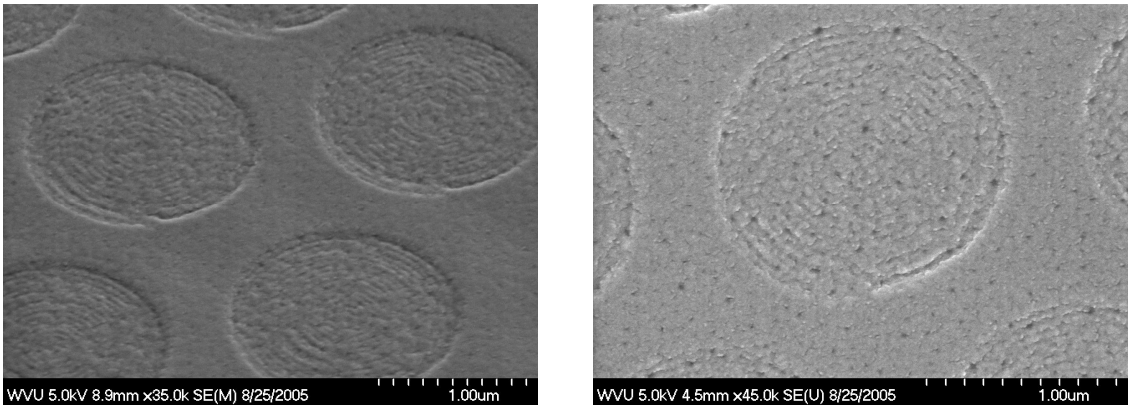

Figure 4.11. SEM images of Pattern 'i', Dose: 250μC/cm^2. (resist thickness 80nm)

Table 4.3 Pattern position on sample2

X-Position ↓ →Y-Position	575	580	585
330	A*		
335	B	C	D
340	G	F	E*
345	H	I	

Table 4.4 Doses for patterns with 'a'=1 microns, and 'r'= 400nms on sample2.

Pattern	Magnification	Dose	Time (In Seconds)
A	647		39.4
B	3.67k	50	2.4
C	3.67k	100	4.6
D	3.67k	150	6.9
E	647		39.4
F	3.67k	200	9.1
G	3.67k	250	11.4

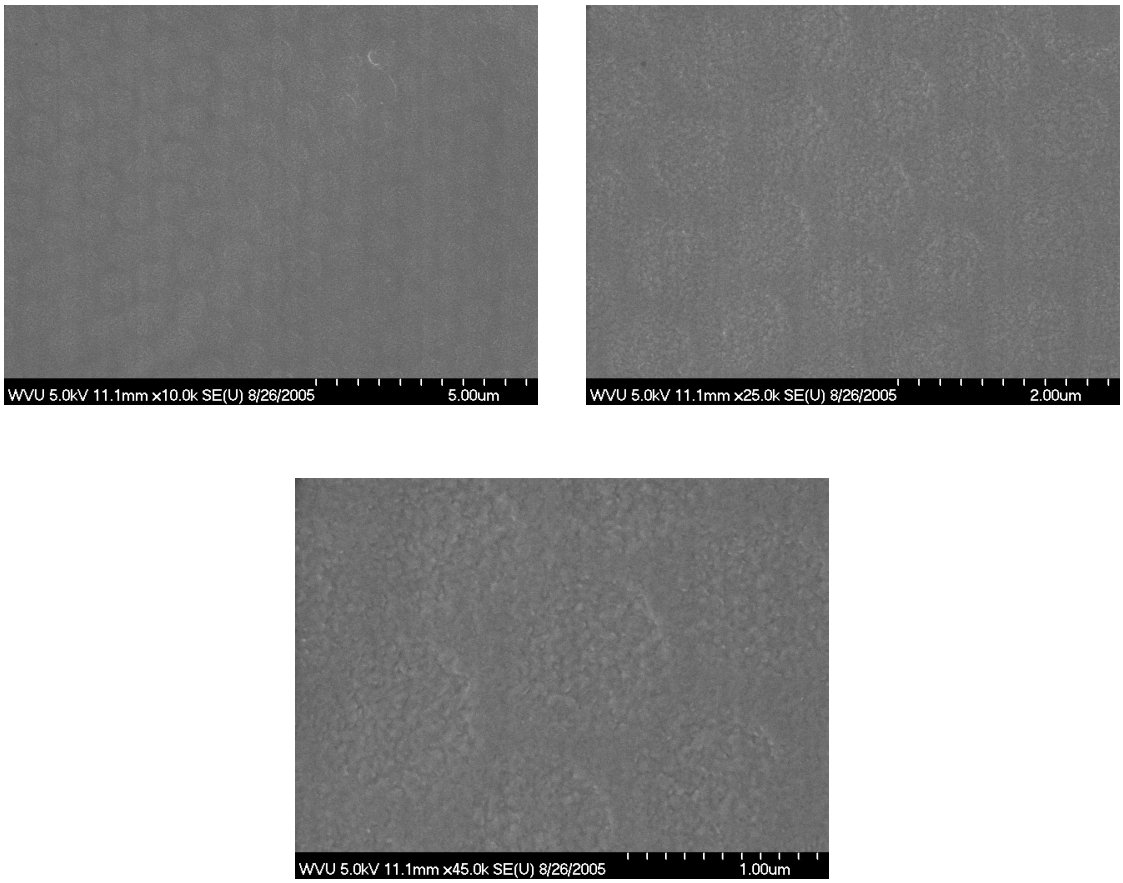

Figure 4.12. SEM images of Pattern 'f' Dose: 200μC/cm^2. (resist thickness 80nm)

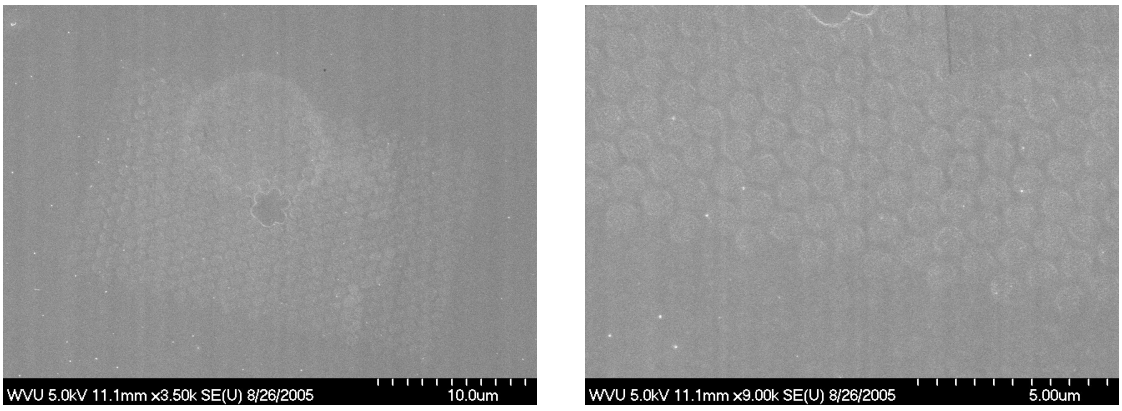

Figure 4.13.SEM images of Pattern 'g', Dose: 250μC/cm^2. (resist thickness 80nm)

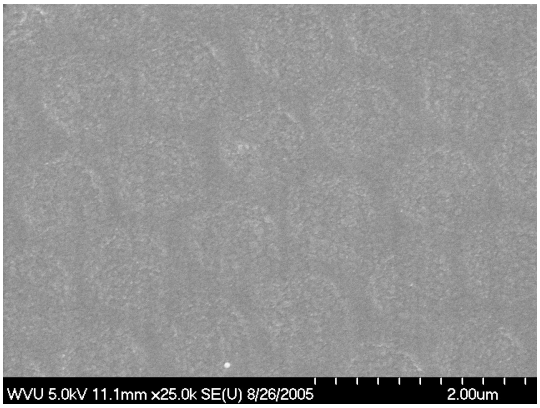

Figure 4.14.SEM image of Pattern 'g', Dose: 250μC/cm^2. (resist thickness 80nm)

The patterns appeared to be underexposed. The same patterns were written again with the same conditions, but higher dose. No pattern was seen under the SEM. The spin program was changed to program 2 in Appendix B. Also the baking time was increased to 75 Seconds from 60 seconds. With this spin program, the patterns were written again.

Table 4.5 Pattern position on sample3

X-Position ↓ →Y-Position	575	580	585
330	a*		
335	B	C	D
340	G	F	e*
345	H	I	J

Table 4.6 Doses for patterns with a=2 microns, and 'r'= 800nm on sample3

Pattern	Magnification	Dose (in μC/cm^2)	Time (in Seconds)
A	647		
B	2.69k	125	10.1
C	2.69k	150	12.1
D	2.69k	175	14.1
E	647		39.4
F	2.69k	200	16.1
G	2.69k	225	18.1
H	2.69k	235	18.9
I	2.69k	245	19.7
J	2.69k	250	20.1

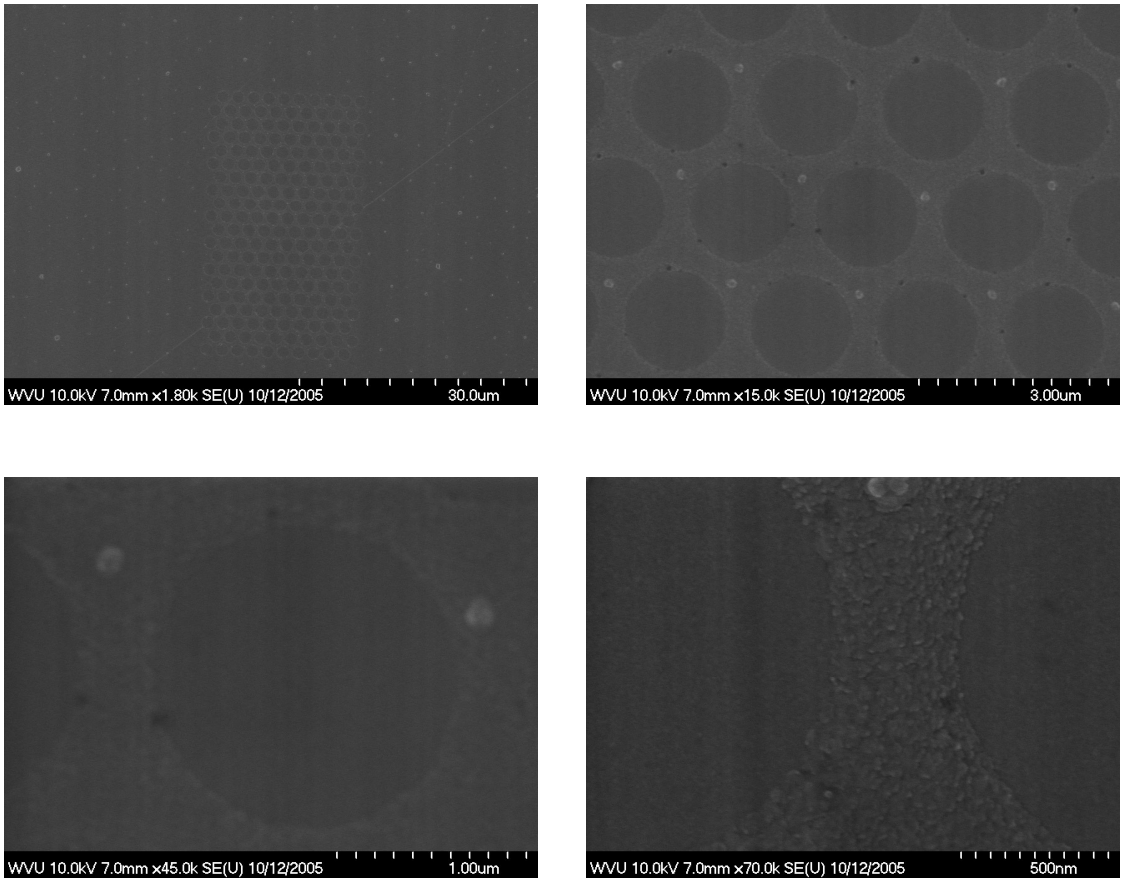

Figure 4.15. SEM images for pattern 'b', dose 125 μC/ cm^2. (resist thickness 80nm)

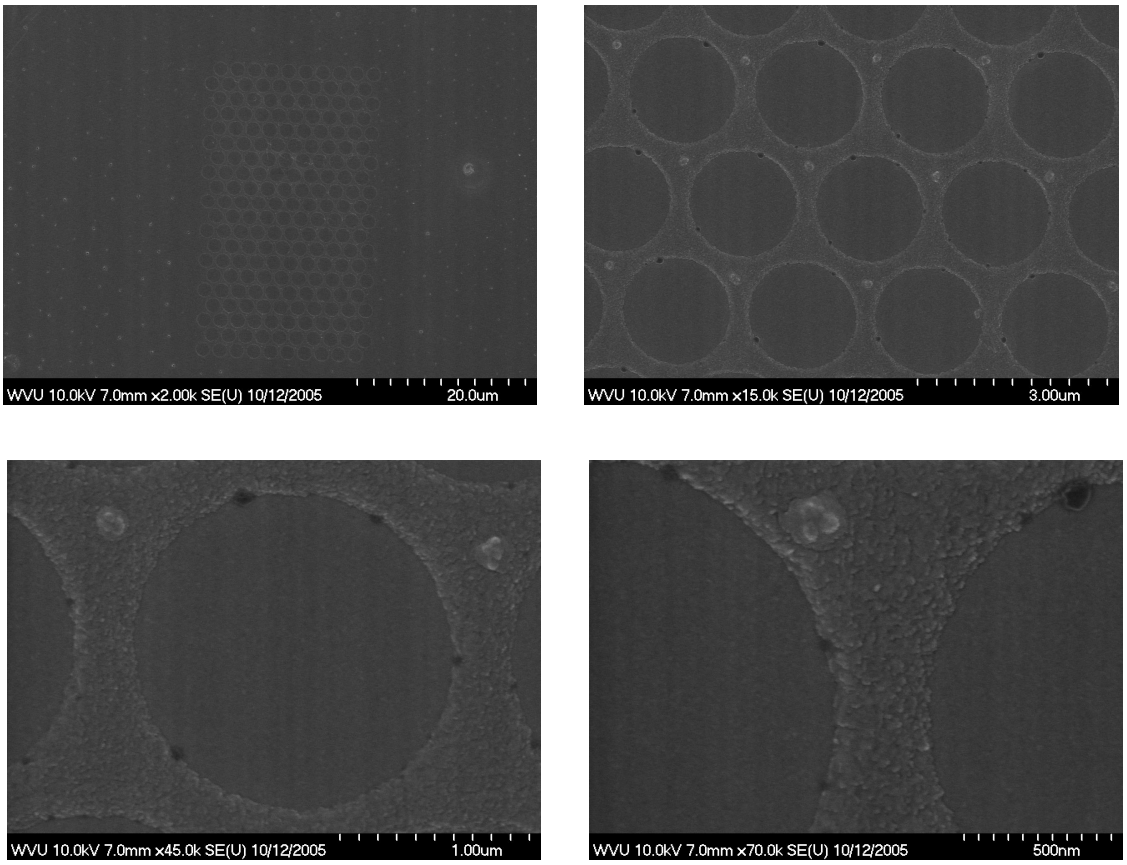

Figure 4.16. SEM images for pattern 'c', dose 150 μC/ cm^2 (resist thickness 80nm)

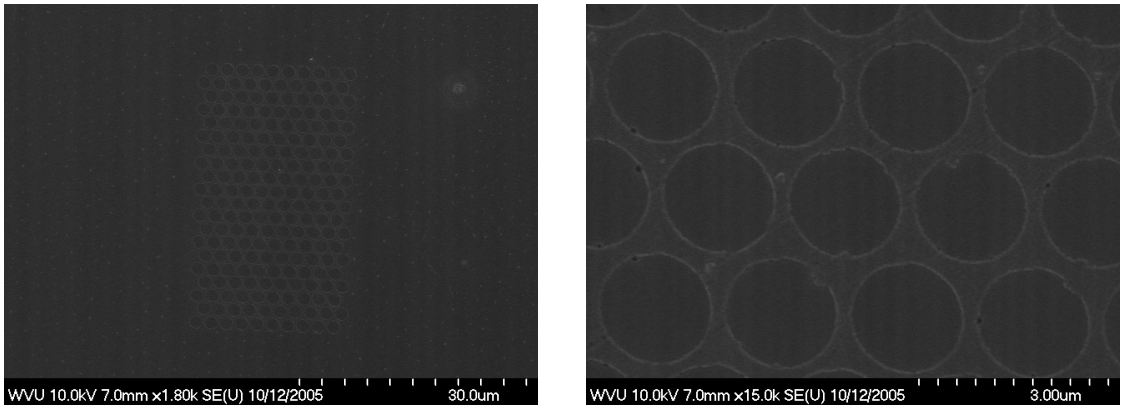

Figure 4.17. SEM images for pattern 'd', dose 175 μC/ cm^2 (resist thickness 80nm)

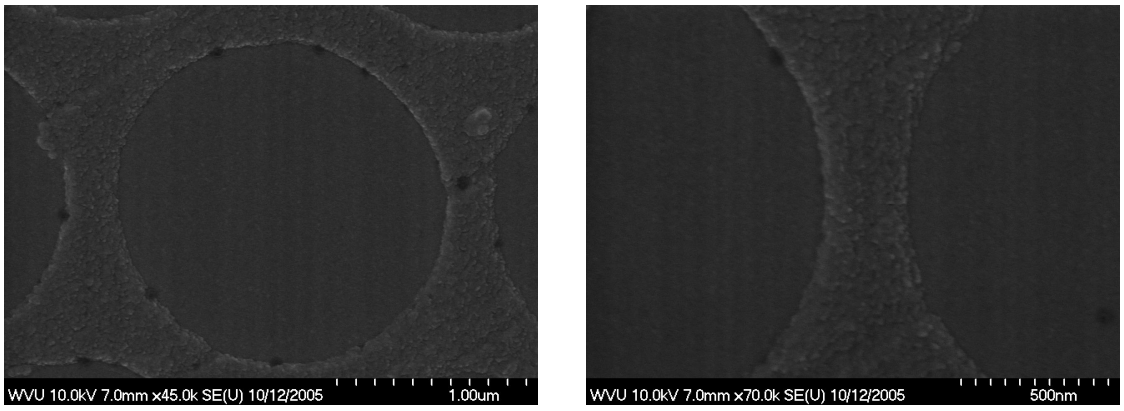

Figure 4.18. SEM images for pattern 'd', dose 175 μC/ cm^2 (resist thickness 80nm)

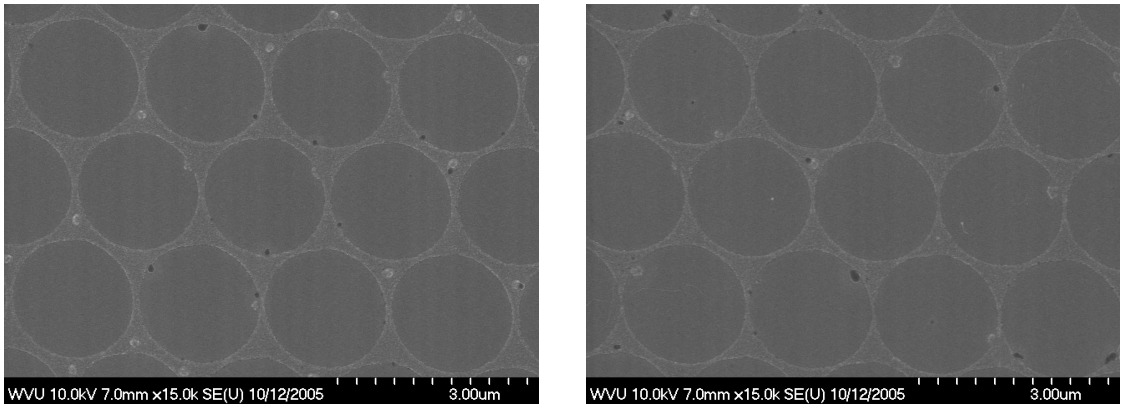

4.19 a 4.19 b

Figure 4.19. SEM images for pattern 'g' and 'h'. 'a' with dose 225 μC/ cm^2 and b with dose 235 μC/ cm^2 (resist thickness 80nm)

The patterns 'b' and 'c' with doses 125 μC/cm^2, and 150 μC/cm^2 were with sizes close to those ideally required. Patterns with doses above those values were over exposed. The best dose for this pattern is around 125 μC/cm^2. The next write was for patterns much smaller than this. These patterns have 'a' 500nms, and 'r' 200nms.

Table 4.7 Pattern position on sample 4

X-Position ↓ →Y-Position	575	580	585
330	A*		
335	B	C	D
340	G	F	E*
345	H	I	

Table 4.8 Doses for patterns with ' a'=500 nm, and 'r'= 200nm on sample 4.

Pattern	Magnification	Dose (in μC/cm^2)	Time (in Seconds)
A	647		39.4
B	5.57k	95	2
C	5.57k	100	2.2
D	5.57k	105	2.3
E	647		39.4
F	5.57k	110	2.4
G	5.57k	115	2.5
H	5.57k	120	2.6
I	5.57k	125	2.7

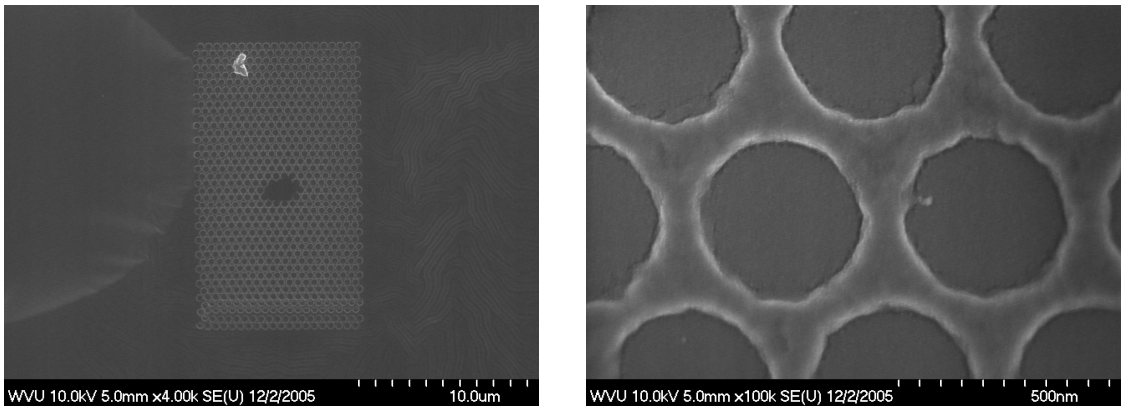

Figure 4.20. SEM images for pattern'b', dose 95 μC/ cm^2

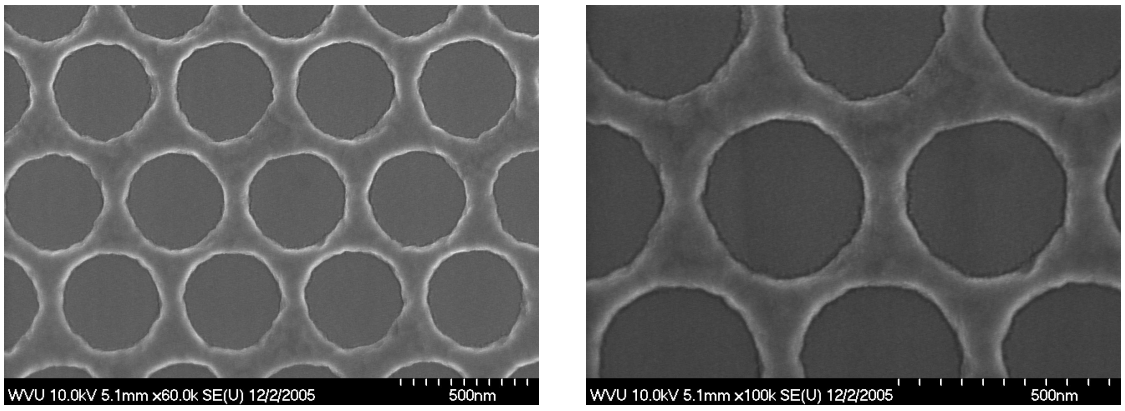

Figure 4.21. SEM images for pattern'c', dose 100 μC/ cm^2 (resist thickness 80nm)

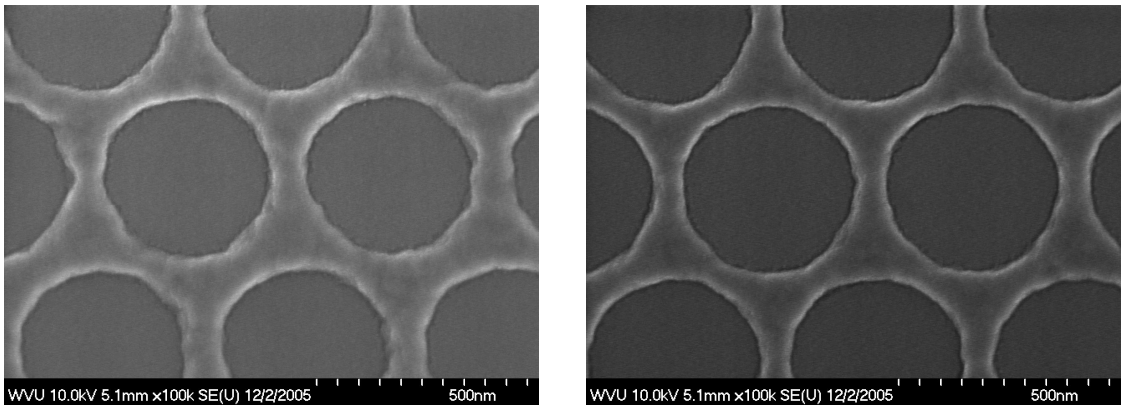

Figure 4.22. SEM images for pattern'd', dose 105 μC/ cm^2 and pattern'h', dose 120 μC/ cm^2(resist thickness 80nm)

Since the pattern here is smaller, the doses should be less than what we tried for bigger patterns. The doses 95 μC/cm^2 and 100 μC/cm^2, are giving patterns close to ideal feature sizes. The doses higher than that were over exposed. The holes were not well defined, at the edges. The patterns were ideal in one direction and were closer than required in diagonal direction. This is due to design of the pattern. The design of the pattern to avoid this is discussed in the next section.

4.4.2. Direct Write on PMMA 950 A4

The PMMA 495 A2 resist is very thin. This thickness of resist is not large enough to mask adequately to etch silicon deep enough. So a much thicker resist should be used.

PMMA 950 A4 can be spun up to 200 nm thick at 4000rpm from the spin speed curves (Figure 4.4). The next sets of writings were done on PMMA 950 A4 resist. The procedure for writing and the writing conditions were same. The dose is again varied to get the patterns close to those required. The pattern size earlier was 20 X 20 microns. It was difficult to identify the patterns under the SEM because of the small size. So to make the identification of patterns easier under the SEM the array size was increased to 50 X 50 microns.

Table 4.9 Pattern position on sample 5

X-Position ↓ →Y-Position	504	509	514
304	B	C	D
309	G	F	
314	H		I
319		J	

Table 4.10 Doses for patterns with a=1 micron, and 'r'= 400nms on sample 5.

Pattern	Magnification	Dose (in μC/cm^2)	Time (in Mins)
B	1.03K	350	2.96
C	1.03K	375	3.17
D	1.03K	400	3.38
E			
F	1.03K	425	3.6
G	1.03K	450	3.81
H	1.03K	475	4.02
I	1.03K	500	4.23
J	1.03K	525	4.44

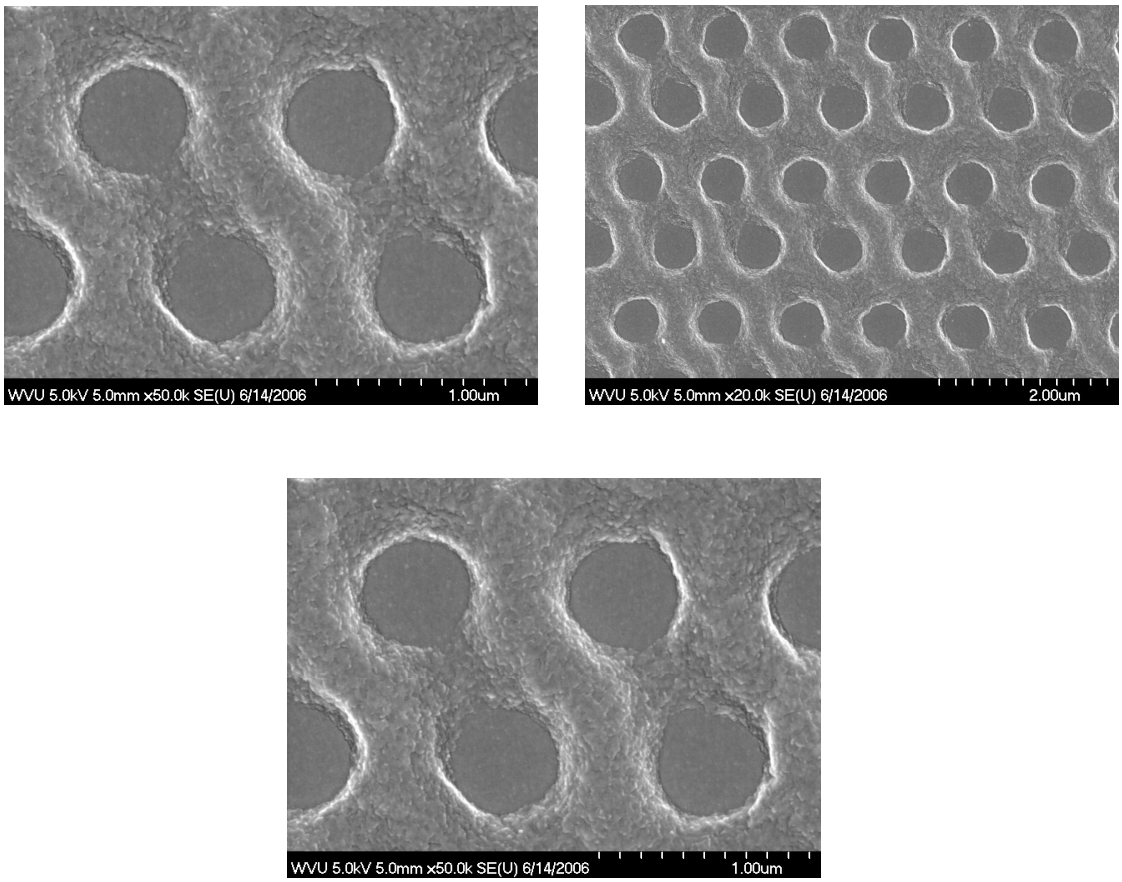

Figure 4.23. SEM images for pattern'b', dose 350 μC/ cm^2 (resist thickness 200nm)

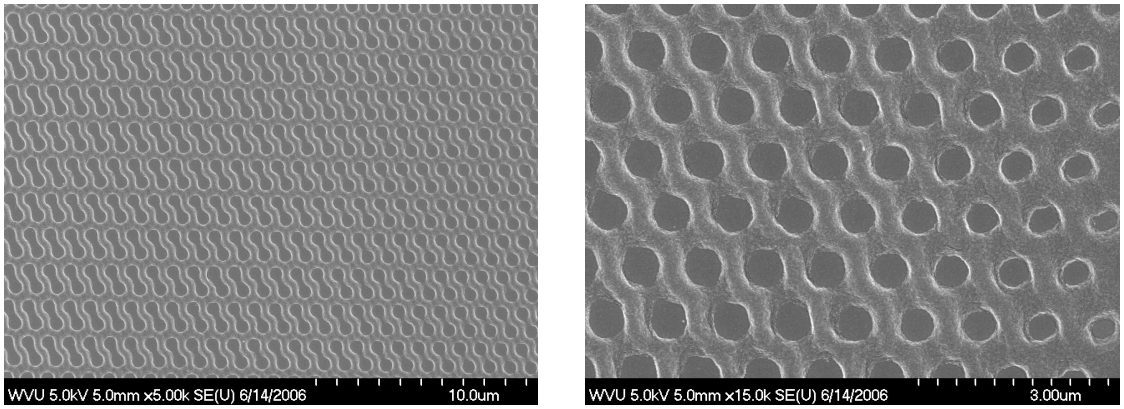

Figure 4.24. SEM images for pattern'c', dose 375 μC/ cm^2 (resist thickness 200nm)

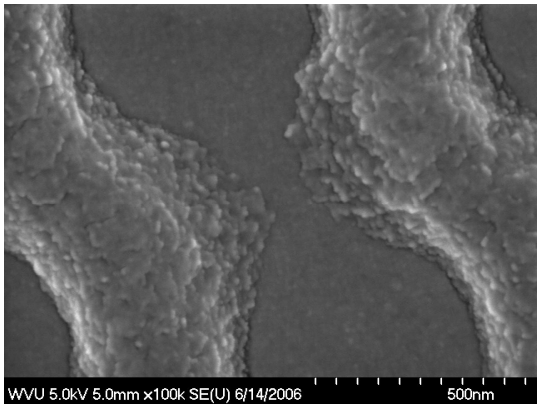

Figure 4.25. SEM images for pattern'c', dose 375 μC/ cm^2 (resist thickness 200nm)

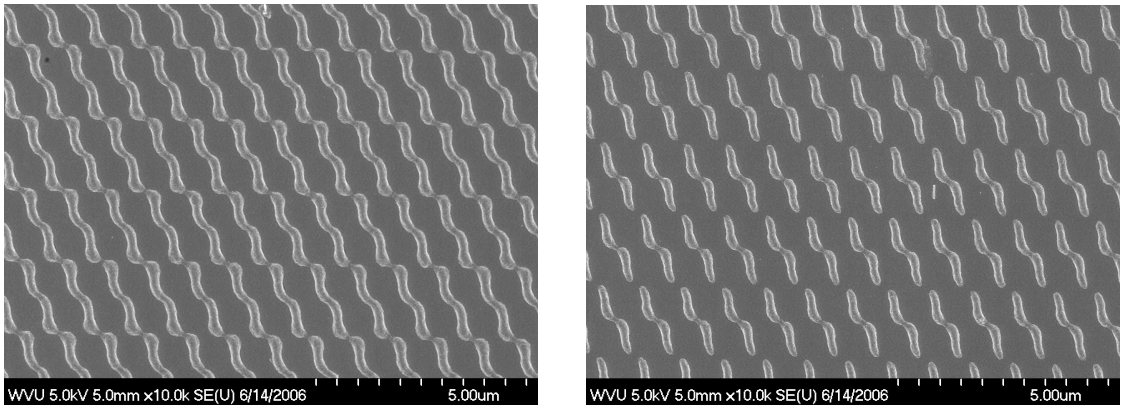

Figure 4.26. SEM images for pattern'h'and 'I', doses 475 μC/ cm^2 and 500 μC/ cm^2 respectively. (resist thickness 200nm)

The patterns for dose 325 μC/ cm^2, and 350 μC/ cm^2 were underexposed, and the doses above that were overexposed, and also the holes in the adjacent lines were mixing with each other.

The same pattern was written again with the same parameters, but with a lower dose again.

Table 4.11 Pattern position on sample 6

X-Position ↓ →Y-Position	506	511	516
307	B	C	D
312	F		E
317	G	H	
322		J	I

Table 4.12 Doses for patterns with a=1 micron, and 'r'= 400nm on sample 6

Pattern	Magnification	Dose (in μC/cm^2)	Time (in Secs)
B	1.8K	310	78.3
C	1.8K	320	80.8
D	1.8K	330	83.4
E	1.8K	340	85.9
F	1.8K	350	88.4
G	1.8K	360	90.9
H	1.8K	370	93.4
I	1.8K	380	98.4
J	1.8K	390	95.9

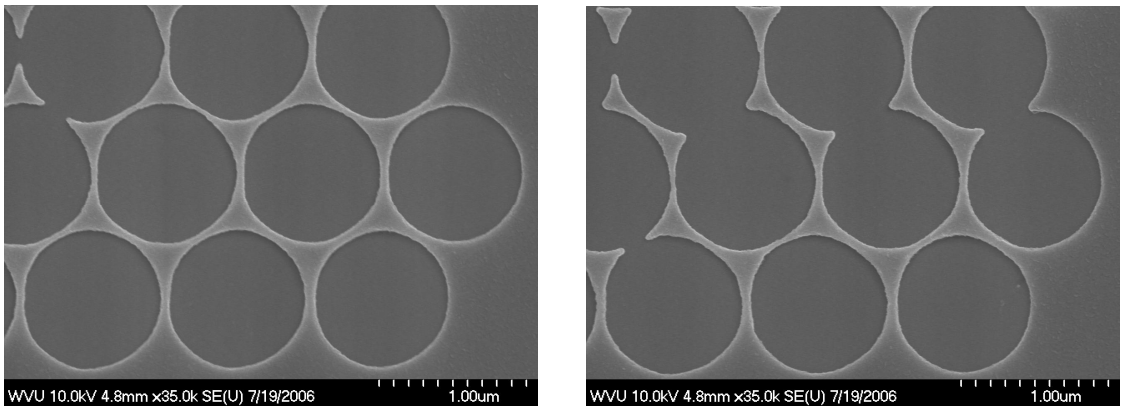

Figure 4.27. SEM images for patterns with doses 310 μC/ cm^2 and 320 μC/ cm^2 respectively. (resist thickness 200nm)

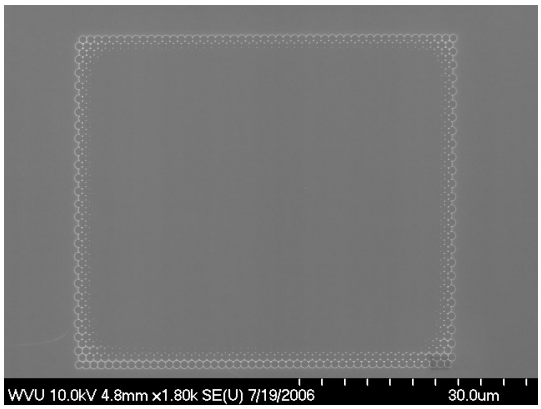

Figure 4.28. SEM images for pattern with dose 380 μC/ cm^2(resist thickness 200nm)

The SEM images for these patterns, contained no pattern at the center and at the outer side of the array, there were few lines of the patterns visible. Also at the edges, the holes again seem to be mixing with each other. The first effect is due to the proximity effect, where the secondary electrons, tend to expose the resist form under the PMMA surface, and also the outer surface of the whole pattern receives lower dose than that of the pattern which is inside. The second effect is due to the design of the pattern. The pattern was designed by creating two sets of dot arrays. One offset with the other to form a triangular array of holes. The beam writes the first array completely in a zigzag fashion and then comes back to the top and starts writing the second array. There might be stage offset or beam offset effects which were possibly creating the mixing effect. The design of the pattern was again changed. The pattern is designed now so that the first two rows of the pattern were written first with an offset. Then these two lines were set to make an array of triangular holes. The proximity effect is avoided by designing holes of smaller radius, and also designing two layers. One layer outside with a higher dose than the layer in center, and other in the center with regular dose. The probe current was changed to a 63.4pA.

Table 4.13 Pattern position on sample 7

X-Position ↓ →Y-Position	495	500	505	510
307	B	C	D	E
312	H	G	F	
317	I		J	

322			K	

Table 4.14Doses for patterns with a=1 micron, and 'r'= 300nm on sample 7

Pattern	Magnification	Dose (in μC/cm^2)		Time (in Secs)
		Outer surface	Center	
B	1.8K	160	150	22.1
C	1.8K	170	160	23.5
D	1.8K	180	170	24.9
E	1.8K	200	180	26.5
F	1.8K	210	190	28
G	1.8K	220	200	29.4
H	1.8K	240	210	31
I	1.8K	250	220	32.5
J	1.8K	260	230	33.9
K	1.8K	160	140	20.8

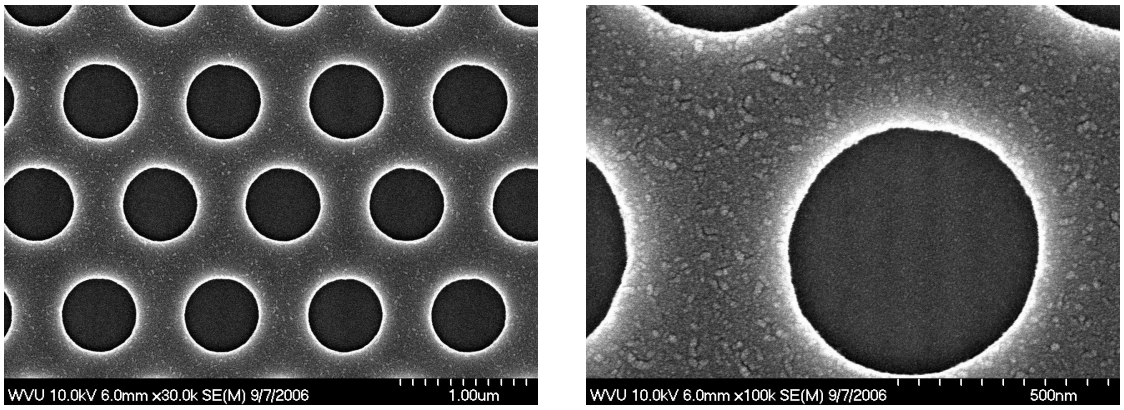

Figure 4.29. SEM images for patterns 'k' with doses 140 μC/ cm^2 and 160 μC/ cm^2 at center and edge respectively(resist thickness 200nm)

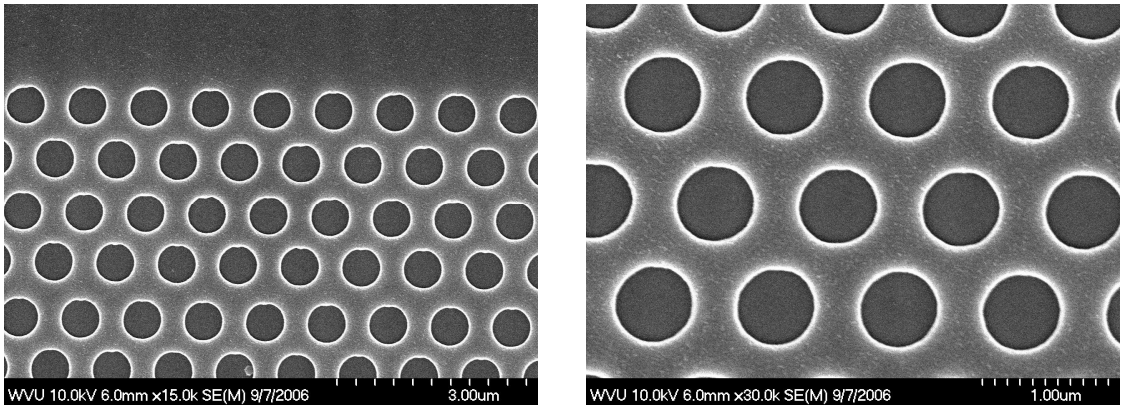

Figure 4.30. SEM images for patterns 'b' with dose 150 μC/ cm^2 and 160 μC/ cm^2 at center and edge respectively(resist thickness 200nm)

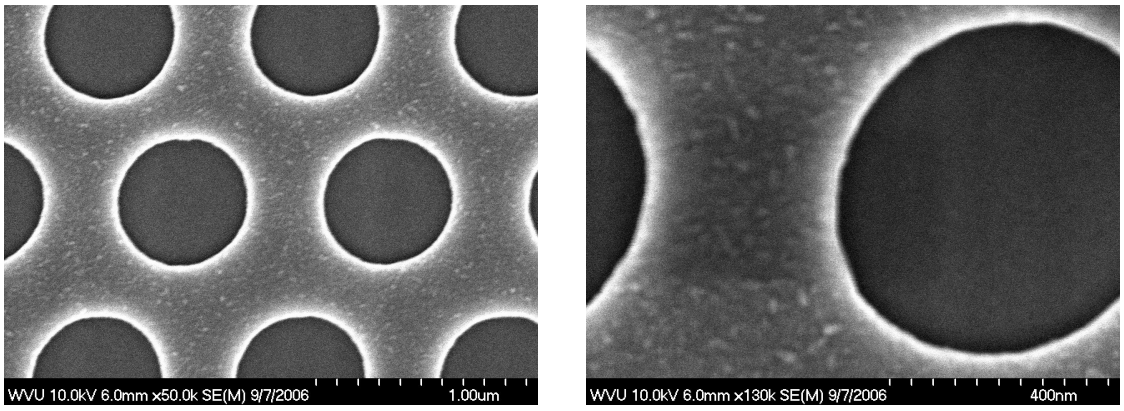

Figure 4.31. SEM images for patterns'd' with dose 170 μC/ cm^2 and 180 μC/ cm^2 at center and edge respectively(resist thickness 200nm)

The patterns with doses with 140 μC/ cm^2 and 150 μC/ cm^2 were the best patterns, with pattern sizes close to what were designed. This design of patterns with 2 layers, containing different doses outside and at the center gave good patterns with no proximity effects. Also the write mode of writing the patterns from top to bottom in a single write did eliminate the problem of holes of adjacent rows mixing with each other.

4.5. Reactive Ion Etching (RIE) of Silicon

The next step in the development of the fabrication process would be the determination of the process to transfer the resist pattern to a hard mask (oxide for example) and then into the photonic crystal layer. Initial experiments for etching of Silicon were done using Inductively Coupled Plasma- Reactive Ion Etching (ICP-RIE). SF_6 gas was used as an etchant for the etching process. The silicon wafer with thermally grown SiO_2 (383 nm thick) was patterned using UV photo lithography with AZ5214 as the resist. The exposed SiO_2 was removed using Buffered Oxide Etch (BOE). The exposed Si surface was then etched using RIE. Parameters for etching were RF power-220W, ICP power -150 W, Pressure 3mTorr, Flow rate of SF_6 -10sccm. The sample was etched for 3 minutes. The residual SiO_2, was removed by performing BOE dip. The samples were analyzed using an SEM. The etch depth was about 1.755 microns. The SEM images are shown in Figure 4.32. This etch process may be useful for effective through-etching needed as part of the silicon photonic crystal fabrication process.

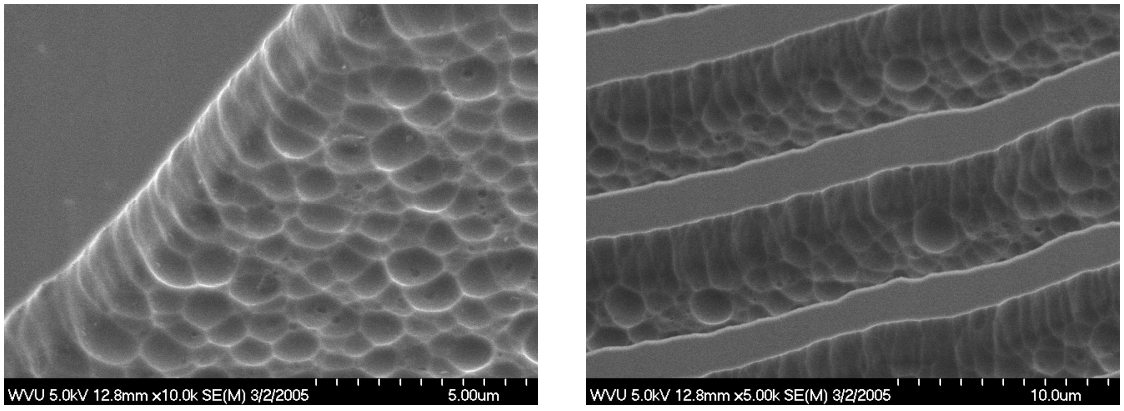

Figure 4.32. SEM images of etched silicon.

CHAPTER V

CONCLUSIONS AND FUTURE WORK

In this research, application of photonic crystal defects for biosensing applications was evaluated. The initial simulation results indicate that the optical properties of the device are very sensitive to the changes in the refractive index of a single defect. The shift in wavelength supported by the defect is about 0.04nm, for change in refractive index of 0.001 for DI water filling holes in a silicon substrate. Results also show that the change in wavelength has increased with the increase in the number of defects for change in refractive index of defect. Results indicate that the shift in wavelength has increased to 0.12nm for 5 defects. The fabrication efforts to develop the initial prototype were also discussed. Efforts to use direct write E-beam lithography to write these patterns on two different PMMA resists on silicon substrate was demonstrated. The photonic crystal patterns with 'a' 500nm and 'r' 200nm were optimized on 80nm thick PMMA 495 A2 resist. The patterns with 'a' 1 micron, and 'r' 300nm were optimized on 200nm thick PMMA 950 A4 resist. The two layer design approach of the patterns using design CAD software was optimized to eliminate the proximity effects.

Future work consists of understanding more fully the complete capabilities of the simulation tool (both 2-D and 3-D), and optimizing the fabrication procedures to obtain the patterns in silicon and GaN substrates. The understanding of different inputs using FDTD tool may be helpful in exploring the complete potential of the PCs for biosensing applications. Simulating a photonic crystal slab structure using 3-D simulations can aid in exploring different possibilities of exploiting the complete band gap effect for biosensing applications. The fabrication procedure of these structures with even smaller pattern sizes needs to be optimized. The efforts of fabricating PC structures in PMMA with GaN as the base substrate need to be explored. The Reactive Ion Etching (RIE) process for etching these patterns in the substrate (silicon and GaN) with PMMA as mask also needs to be explored further and implemented with the e-beam pattern developed through this work. These future efforts would further aid the research progress in realizing a biosensor for near-infrared and visible range of wavelengths using photonic crystals.

BIBLIOGRAPHY

[1] Introduction to Bio photonics Paras N.Prasad.John Wiley and sons, 2003.

[2] Sheng-Hong Yu, Cheng-Hau Chen, Huihua Kenny Chiang, *"Fiber Optic evanescent eave biosensor for biomolecular detection"*, IEEE , Second Asian and Pacific Rim Symposium on Biophotonics, 2004.

[3] Tzyy-jiann Wang, Cheng-Wei Tu, Fu-kun Liu, and Hsuen-Li Chen, "*Surface Plasmon Resonance Waveguide Biosensor by Bipolarization Wavelength Interrogation",* IEEE Photonics Technology Letters Vol.16.No.7, July 2004.

[4] Joel P.golden, George P.Anderson, Sina Y.Rabbany, and Frances S.Ligler, "*An Evanescent Wave Biosensor-Part II : Fluorescent Signal Acquisition from Tapered Fiber Optic probes"*, IEEE Transactions on Biomedical Engineering"

[5] E.Yablonovitch, "*Inhibited Spontaneous Emission in Solid State Physics and Electronics* ", Physical Review Letters, **Vol.58**, No.20, pp 2059-2062, 18 May 1987.

[6] S.John, "*Strong Localization of Photons in certain disordered Dielectric Superlattices*", Physical Review Letters, **Vol.58,** No.23, pp 2486-2489, 8 June 1987.

[7] Steven G.Johnson, John D.Joannopoulos, Photonic Crystals: The road from theory to practice- Springer

[8] E.Chow, A.Grot, L.W.Mirkarimi, M.Sigalas, and G.Girolami, *"Ultracompact biochemical sensor built with two-dimensional Photonic Crystal microcavity"*, OPTICS LETTERS, **Vol.29**, No.10, May 15, 2004.

[9] Hamza Kurt, and D.S.Citrin, *"Photonic crystals for biochemical sensing in Terahertz region"*, Applied Physics letters, **Vol.87**, 041108, 2005.

[10] David Erickson, Teresa Emery, Troy Rockwood, Axel Scherer and Demetri Psaltis, *"Integration of sub-wavelength nanaofluidics with Photonic crystals",* Proceedings of IMECE , ASME International Mechanical Engineering Congress and Exposition, 2005.

[11] T.Yoshie, O.B.Shehekin, H.Chen, D.D.Deppe and A.Scherer "*Quantam dot photonic crystal lasers*", Electronics letters, Vol. 38, No. 17, 15th August 2002.

[12] Jonathan J. Wierer, Michael R. Krames, John E. Epler, and Nathan F. Gardner, Joel R. Wendt, Mihail M. Sigalas , Steven R. J. Brueck and Dong Li , Michael Shagam, *"III Nitride LEDs with Photonic Crystal structures"*, Proceedings of SPIE -- Volume 5739, 2005.

[13] Masaya Notomi, Akihiko Shinya, Satoshi Mitsugi, Goh Kira, Eiichi Kuramochi, and Takasumi Tanabe, *"Optical bistable switiching action of Si high-Q photonic-crystal nanocavities",* Optics Express, Vol.13, No.7, April 2005.

[14] Masatoshi Tokushima, Hideo Kosaka, Akihisa Tomita and Hirohito Yamada, "*Lightwave propagation through a 120^o sharply bent single line defect photonic crystal waveguide"* Applied Physics Letters, Vol.76, No.8, February 2000.

[15] Terence J. Shepherd, Charlotte R. Bennett, David M. Taylor, and Laurent F. Michaille, *"High channel density optical interconnects using photonic crystal fibers",* Proceedings of SPIE, Volume 6126, 2006.

[16] NanoPhotonics- Paras N.Prasad, Wiley.

[17] Photonic Crystals: Molding the Flow of Light -John D.Joannopoulos, Robert D.Meade, Joshua N.Winn, Princeton.

[18] K.Inoue, K.Ohtaka, Photonic Crystals: Physics, Fabrication and applications-Springer.

[19] Steven G.Johnson and J.D. Joannopoulos, *"Iterative frequency-domain methods for Maxwell's equations in a planewave basis* ", Optics Express **8**, no.3 173-190, 2001.

[20] www.optiwave.com

[21] Kane S.Yee, *"Numerical solution of Initial Boundary Value Problems Involving Maxwell's Equations in Isotropic media",* IEEE transactions on Antennas and propagation, **Vol.14,** issue 3, 302-307, May 1966.

[22] Opti FDTD Technical Background and tutorials, Version 6.0.

[23] K.B.Crozier, S.Kim, O.Kilie, W.Suh, S.Fan, and O.Solgaard, *"Two-Dimensional Photonic Crystals at visible Wavelengths",* Conference on Lasers and Electro-optics (CLEO), 2004.

[24] Marko Loncar, Theodor Doll, Jelena Vuckovic, and Alex Scherer, *" Design and Fabrication of Silicon Photonic Crystal Optical Waveguides"* Journal of Lightwave Technology, Vol.18, No.10, October, 2000.

[25] Eli Yablonovitch, *"Photonic Crystals: Semiconductors of light"*, Scientific American, 2001.

[26] Wim Bogaerts, Vincent Wiaux, Stephen Beckx, Bert Luyssaert, Peter Bienstman and Roel Baets, *"Fabrication of Photonic Crystals in Silicon-On-Insulator Using 248-nm Deep UV Lithography",* IEEE Journal of Selected Topics in Quantam Electronics, **Vol. 8,** No.4, July/August, 2002.

[27] P.K.Montgomery *et al*.,"*High NA ArF Lithography for 70nm technologies",* Proc. Optical Microlithography XV, SPIE 2002, **Vol. 4691**.

[28] www.microchem.com

[29] Erica Bennici,"*Amorphous silicon based Photonic Crystals"* Doctorate thesis, Polytechnic of Turin.

[30] M. A. McCord and R. Michael J. Electron beam lithography. "*Handbook of Microlithography, Micromachining and Microfabrication"*, volume 1. SPIE Press, Bellingham - Washington, 1997.

[31] www.jcnabity.com.

[32] Divya Pishorty, "*Investigation of fabrication process development for integrated optical grating structures*" Masters Thesis, West Virginia University.

APPENDIX A

A.1. SIMULATION PROCEDURE

Steps for using the OPTI FDTD software.

1. Open the OptiFDTD designer. Click new to start designing the structure.
2. Initial properties tool box opens up as shown in figure.
3. Set the channel profile, and width. Set the wafer dimensions. Since the structure we want to design is air holes in dielectric. The channel profile for silicon or GaN is selected
4. To run 2-D simulation set the 2-D wafer properties, and for 3-D simulations set the 3-D wafer properties. The materials to be used are specified here.
5. The material properties like refractive index values are given using profile designer toolbox.

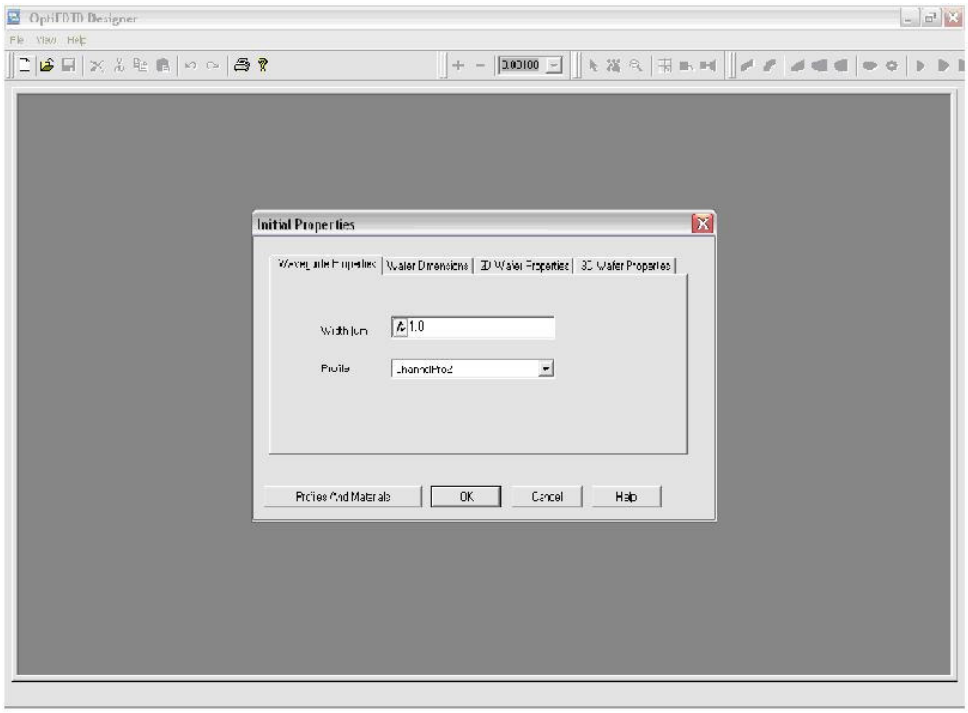

Figure 1: Initial properties dialog box

Profile designer toolbox is used to set the refractive index of materials we want to use to design, the photonic crystal lattice and the defects we want to set in the lattice. Profile designer tool bar is as shown in figure 2.

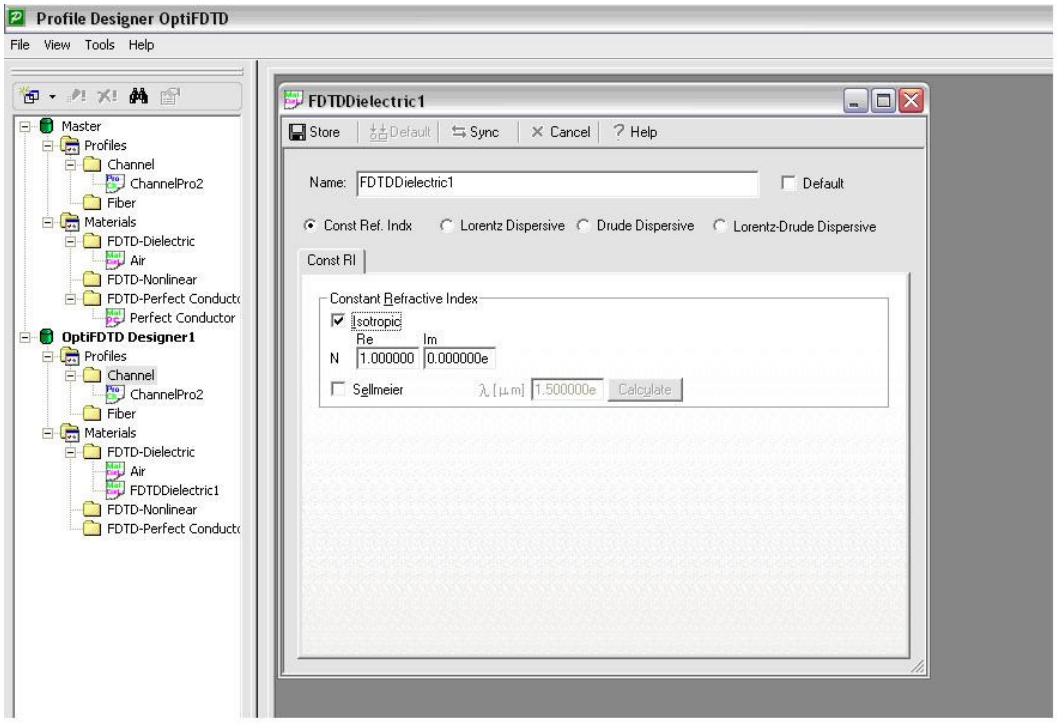

Figure 2. Profile designer toolbox

- Material properties are set using this tool bar. The refractive index value is given and the material type is selected (Isotropic in our case).
- The properties of different materials for the lattice and the defects should be specified here.

After specifying the materials, the channel properties are to be set. The channel profile properties are specified using the channel drop menu.

- Channel profile properties are set by selecting profile-> new. The 2-D or 3-D properties of the channel are set here. The channel properties like width, thickness (for 3-D), and the material to be used (refractive index) are specified here. Figure 3 shows the snap shot of channel profile designer.

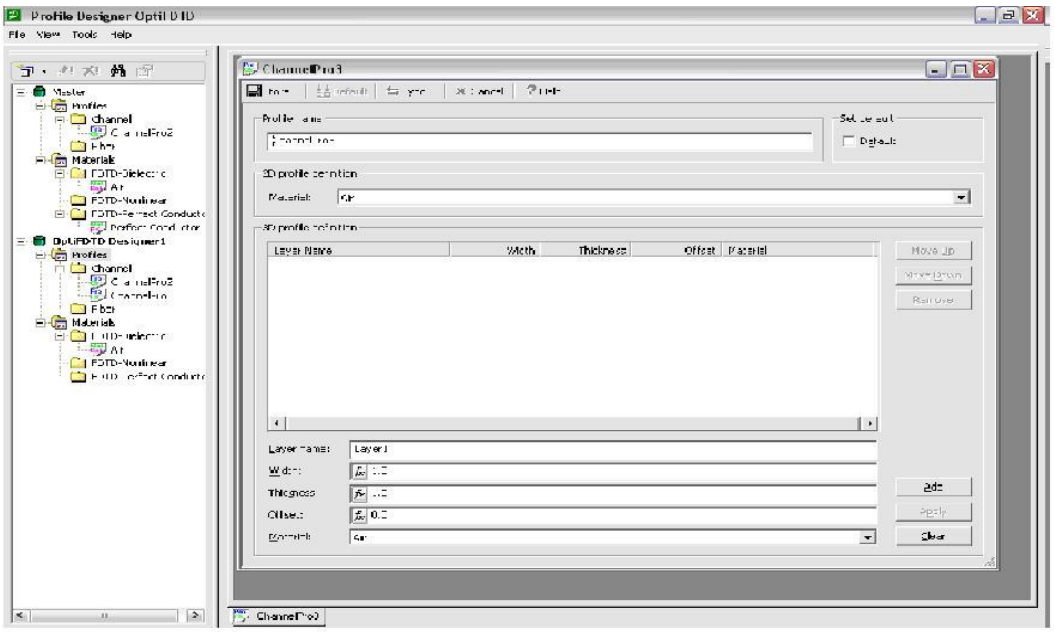

Figure 3. Profile designer toolbox with channel properties window.

The properties of all the materials were specified. The actual structure (photonic crystal) with all the lattice parameters, and radius of each hole are specified using the crystal lattice properties dialog box. Figure 4 shows the snap shot of crystal lattice properties dialog box.

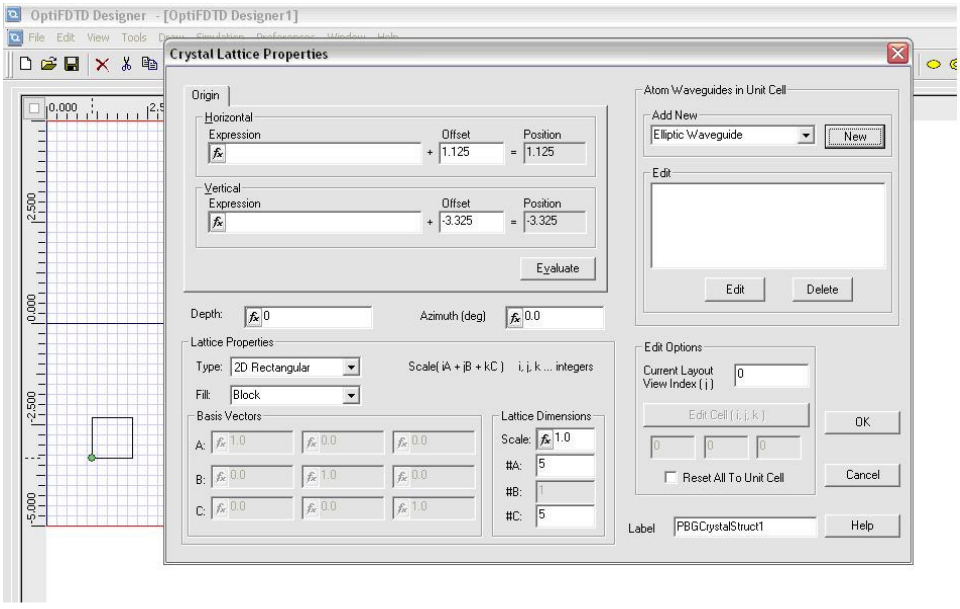

Figure4. Crystal lattice properties dialog box.

- From draw menu select PBG crystal structure. Crystal properties dialog box opens up.
- The lattice properties were specified here. The lattice structure we want to design is the triangular array of holes. The 2-D hexagonal structure is selected.
- The lattice dimensions and the size of the structure will be specified here. The lattice dimensions in A (x-axis), B (y-axis), and C (z-axis) should be give here. For a 2-D simulation lattice dimensions along A and C can only be specified, since the structure is laid in X-Z plane. For a 3-D simulation, the dimensions along C direction should also be specified.

After specifying the lattice properties, the properties of each atom are to be set. Select new from atom wave-guide in unit cell and set the properties of the individual atoms. Since the unit cell here is a circular hole the major radius and minor radius are equal. The material for each atom is also selected here. The material selected here is DI water, whose refractive index should be specified in the profile designer toolbox.

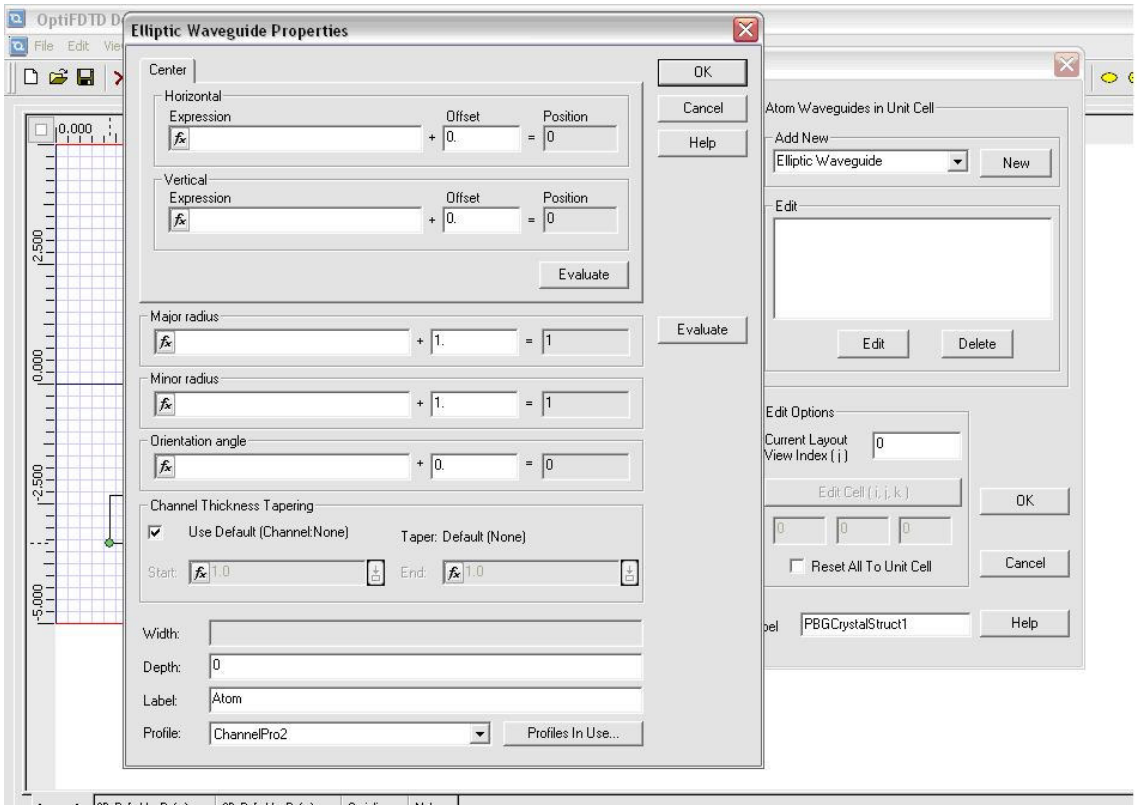

Figure5. Atom wave guides in unit cell dialog box.

Figure 5 shows the atom wave guides in unit cell dialog box, where the properties for individual atoms are specified.

After all the properties for materials in crystal, Lattice dimensions were specified the structure appears as shown in figure 6

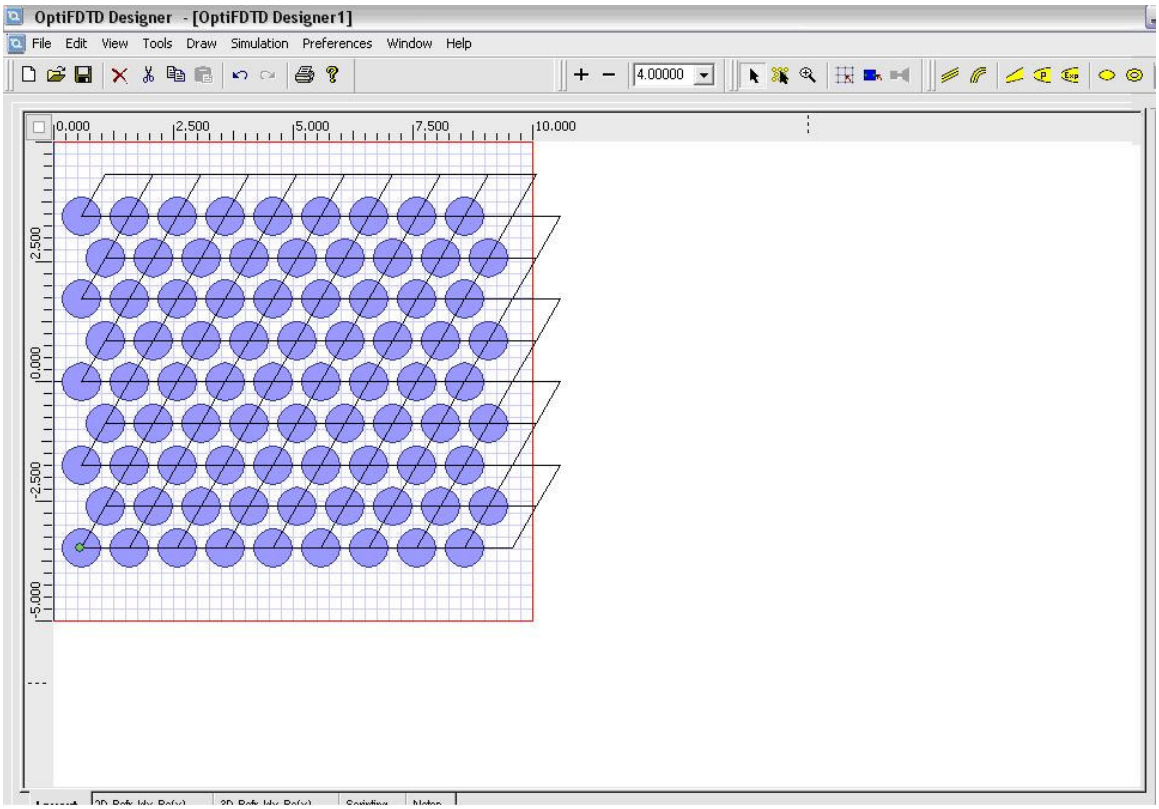

Figure6. Crystal structure for designed parameters.

The properties of the input field are specified using the input field dialog box. There are different types of input and different sources. Continuous wave type, Gaussian modulated continuous wave. The wavelength and amplitude of the input field is specified here. A point source also can be given as input. Figure 7 shows the input field properties dialog box. The simulation is run using 2-D simulation parameters (for a 2-D simulation). Figure 8 shows the simulation parameters dialog box, where the simulation parameters, such as polarization, mesh size and time steps for simulation to run are specified.

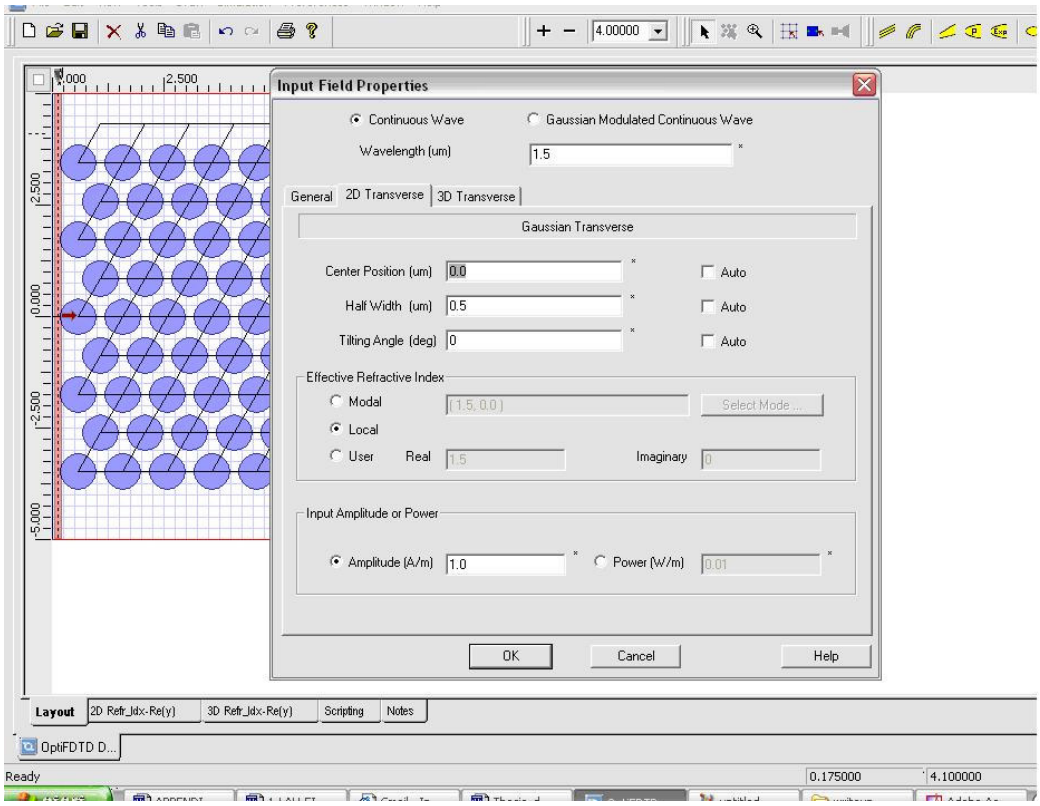

Figure7.Input field properties dialog box.

.

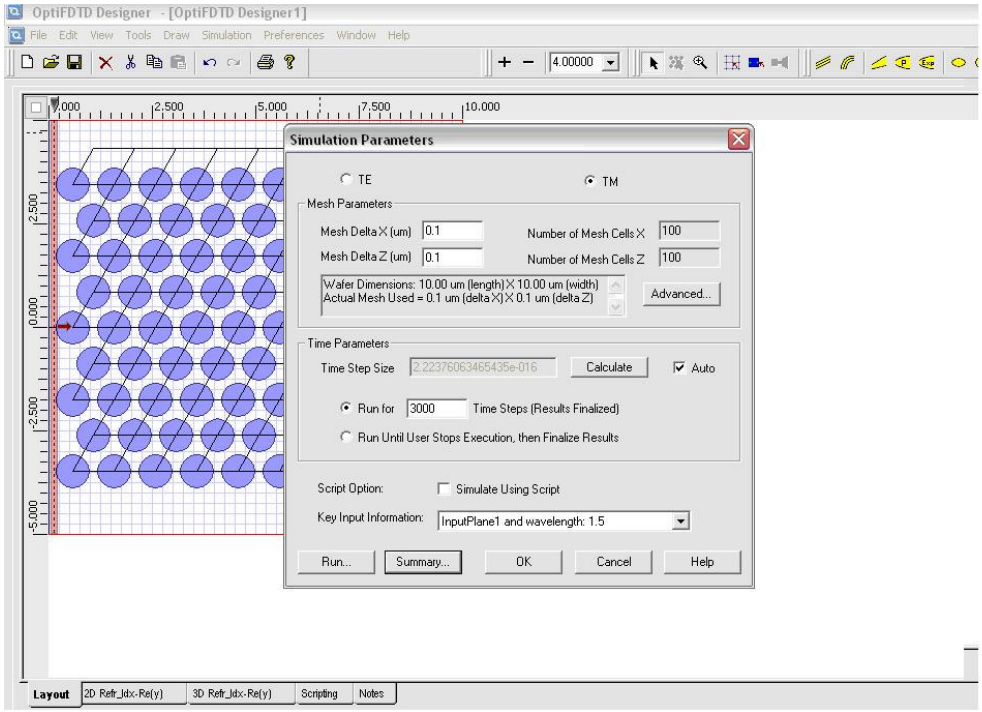

Figure8.Simulation parameters dialog box

We can also set observation point, observation line and observation area, at specified regions, to observe the properties of the crystal after the simulation is run.

Creating defects

Editing each cell can create defects. Click the PBG crystal cell-editing tool and change the properties of each atom. Then right click on the structure at the unit cell, where defect is to be introduced. Click on the cell properties and edit the properties of that unit cell. The refractive index, shape, and size of this unit cell can be changed here. To create a wave guide defect, a line of cells needs to be modified. Figure 9 shows the PBG crystal structure cell editing tool.

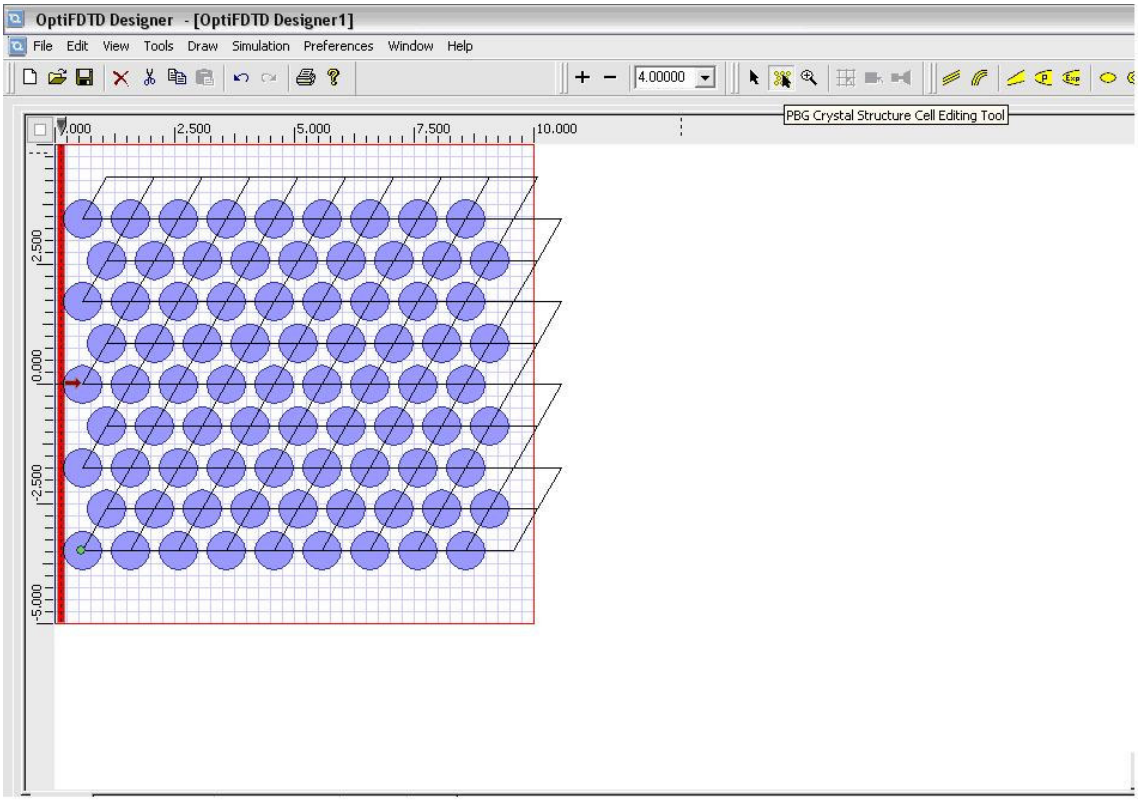

Figure9.PBG Crystal cell editing tool

The run procedure for simulation is same as stated above. After the simulation is run an analyzer file is created. The analyzer file gives the information about the field properties, optical properties of the crystal, and the field patterns at the specified observation points, lines or areas.

A.2. Design Procedure using Design CAD tool for Lithography.

Design CAD LT is a tool used to design patterns for NPGS software. Direct write lithography uses these designed patterns to write the patterns on the resist.

Steps for using Design CAD tool.

1. The DA (Dot Array) option in the NPGS menu is used to create dots of specified radius.
2. Click DA in NPGS menu. Click ‘o’ to make dots as big as circles.
3. A window is popped out asking for the center of the array. Specify the center of array, diameter of each hole, number of columns in each array, column spacing, number of rows in the array, and row spacing. Figure 10 shows the snap shot of the window.
4. A rectangular array is created. But the pattern to be designed is a hexagonal array.
5. To create a Hexagonal array, another array offset from the first array (rectangular array) is created.

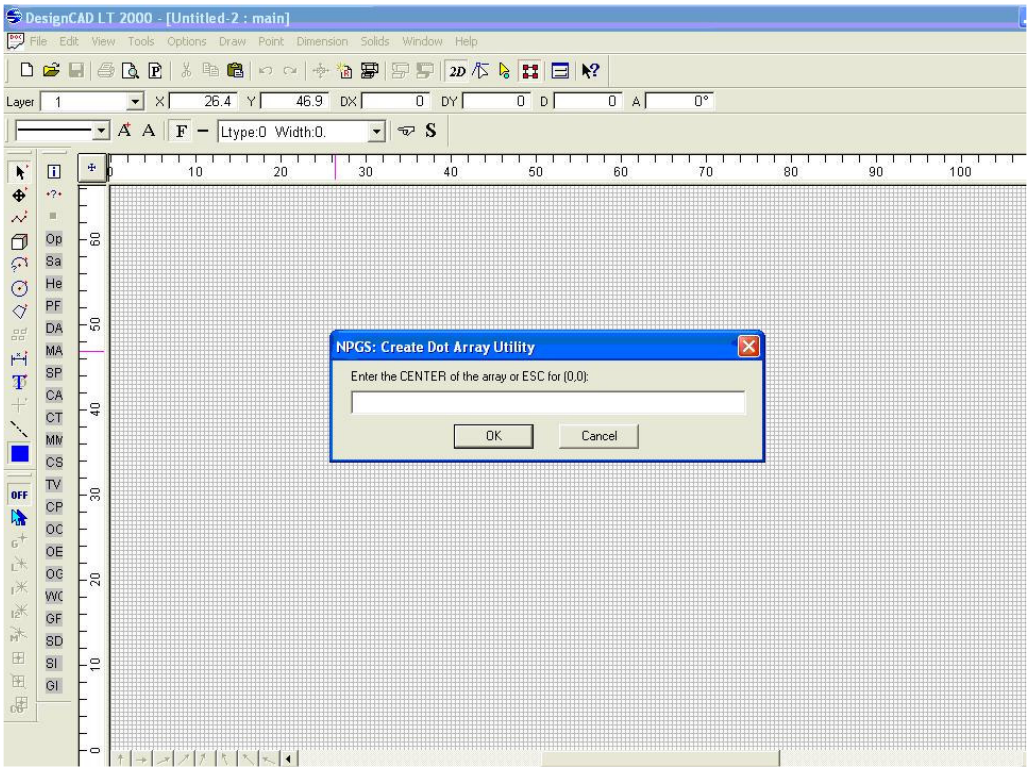

Figure10.Sanp shot of Design cad LT window

The pattern created is as shown in figure 11

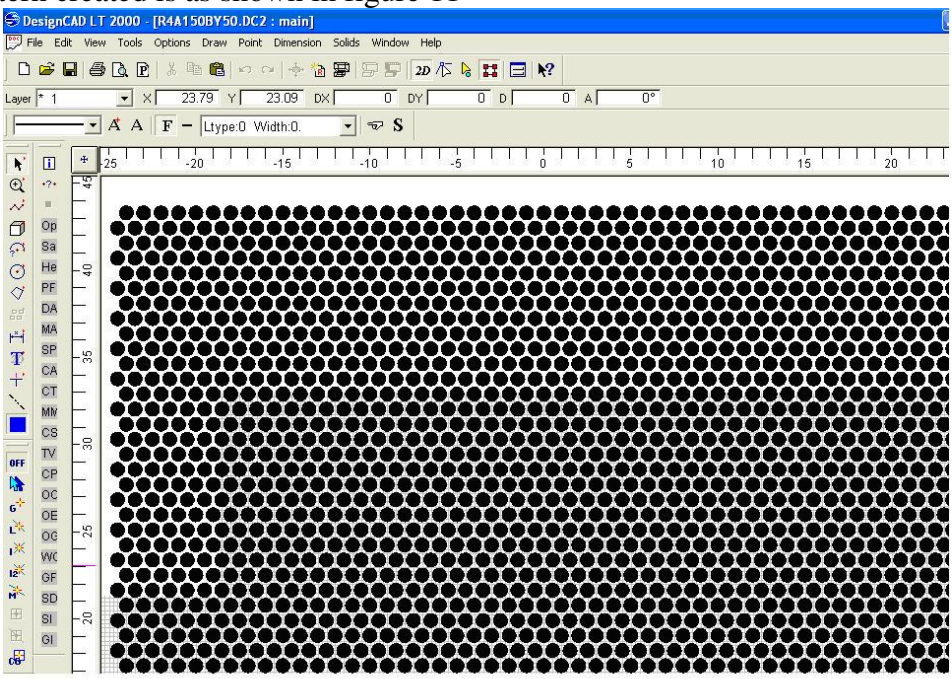

Figure11.Hexagonal pattern created using two rectangular arrays with offset.

The beam by default writes the patterns in the order of creation. SO since the pattern was designed by creating two rectangular array of holes offset with each other to form a hexagonal array, the beam writes the first array from top to bottom and then comes back to top and writes the second pattern from top to bottom. This created a stage offset or beam offset, which resulted in mixing of holes in adjacent rows.

To eliminate this problem, the patterns were designed in such a way so that the hexagonal array is written from top to bottom in one scan. The first two rows were designed, and the write pattern is designed to write the patterns in top row in one direction and continues the writing of second row in the other direction. OE (order entities) option from NPGS menu is used to order the write pattern in the specified fashion. OE option is clicked and a window prompts to select the first entity in the pattern to be designed. The entities should be selected in the order, which we want them to be written. The beam writes the pattern in a zigzag fashion starting form one row to other. The MA (make array) option form NPGS menu is selected to create an array of the first two rows. OC (order check) option enables us to check the order of writing of the pattern.

To eliminate the proximity effects, the patterns were designed in two layers. The dose for each layer can be specified. The outer layer is first designed and then the layer is changed using the options menu. Second layer is then designed. The write pattern here is specified in similar way as explained above (zigzag fashion from top to bottom for first layer and then for second layer). Different doses can be specified for different layers when the writing is done before creating the run files. Figure 12 shows the pattern designed for 2 layers

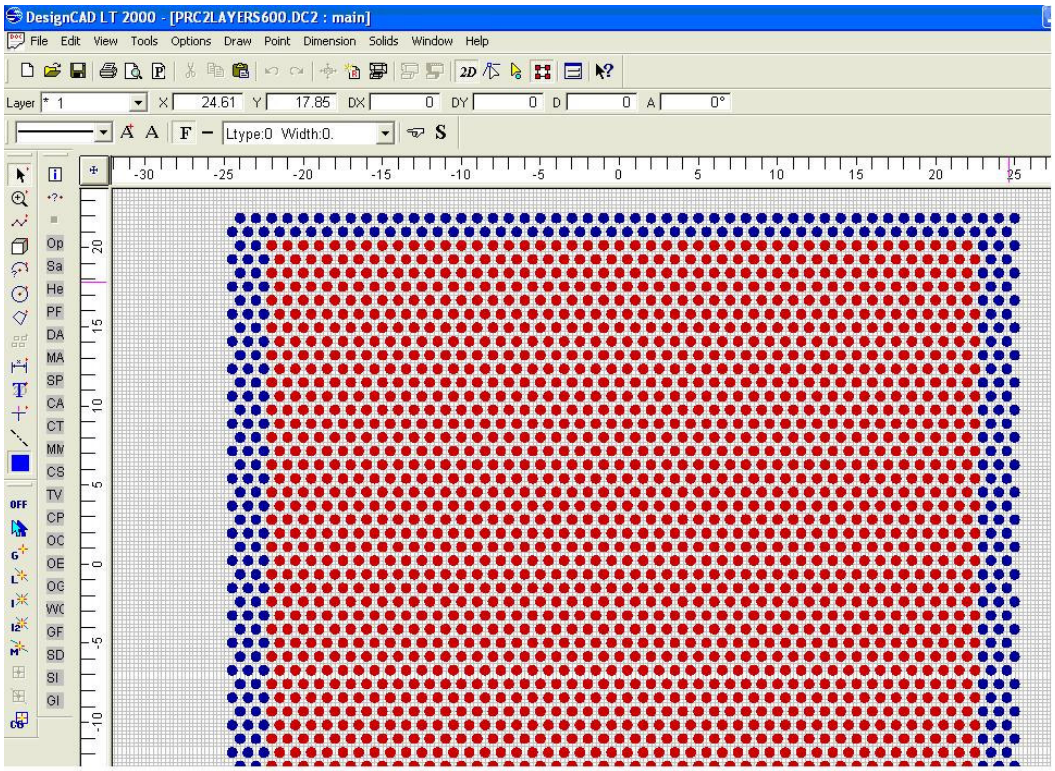

Figure12.Hexagonal pattern created with 2 layers. Different colors specify different layers.

APPENDIX B

B.1. PMMA deposition Spin programs

B.1.1. Resist: PMMA 495 A2

Program1:

1. Sample is placed on the spinner, and spun for 30 seconds at 5000 rpm. Clean with Acetone for first 5 seconds, and then with Methanol for 5 more seconds, and spin dry for next 20 seconds.
2. A clean glass pipette was used to apply the photo resist. The quantity of the resist should be enough to cover the sample.
3. Spin at 500 rpm for 14 seconds first and then accelerate to 4000 rpm speed and spin at final speed of 4000 rpm for 55 seconds.
4. Bake the sample at 180 degrees centigrade temperature for 60 seconds on hot plate.

Program 2:

1. Sample is placed on the spinner.
2. A clean glass pipette was used to apply the photo resist. The quantity of the resist should be enough to cover the sample.
3. Spin at 500 rpm for 7 seconds first and then accelerate to 4000 rpm speed and spin at final speed of 4000 rpm for 55 seconds.
4. Bake the sample at 180 degrees centigrade temperature for 75 seconds on hot plate.

B.1.2. Resist: PMMA 950 A4

1. Sample is placed on the spinner.
2. A clean glass pipette was used to apply the photo resist. The quantity of the resist should be enough to cover the sample.
3. Spin at 500 rpm for 7 seconds first and then accelerate to 4000 rpm speed and spin at final speed of 4000 rpm for 55 seconds.

4. Bake the sample at 180 degrees centigrade temperature for 75 seconds on hot plate.

B.2. Steps for using Direct write E beam Lithography:

1. Place the sample in SEM. Pump down to ultra high vacuum. Rotate the stage so that the copper grid is under the beam. Note the rotation of the sample holder on which the sample is placed.
2. When the system is pumped down to ultra high vacuum, PC is switched on. Insert floppy and then press OPERATE switch to turn ON the E beam machine. Make sure the floppy is inserted before switching the E beam machine ON.
3. Adjust the beam so that it is at the center of the screen. Adjust the filament current so that the beam is circular. Note the Filament current at this beam position.
4. Click 'Emission Image' to see the copper grid. Adjust brightness focus and contrast on the copper grid.
5. Increase the EHT voltage slowly to 30 KV.
6. Adjust the probe current to 49.99 pA.
7. Adjust focus at the magnification required on the copper grid. Adjust astigmatism.
8. Switch on the beam blanker.
9. Move the stage to sample edge and adjust focus on the sample at the magnification required.
10. Switch to software mode.
11. Open the patterns created using Design Cad (Appendix A) in .dc2 extension. Set the probe current, magnification, and area dose ($\mu C/cm^2$) and save as run file (.rf6 extension).
12. Move the stage to the sample center and run programs to write the sample.
13. Note the Dose, exposure time, field size.
14. After writing, vent the chamber, and remove the samples carefully.

B.3. Sputtering

The sample is sputtered with Platinum (Pt) (40nm thick), to vies the patterns under the SEM

1. The sample is mounted and cleaned using N_2.
2. Chamber is opened using 'HOIST UP'. Sample is placed above the Pt target.
3. Mech pump is turned on, and rough valve is opened.
4. The Mech pump is turned off after the chamber pressure goes down to 1.
5. Turn the HVAC (high vacuum) on.
6. Chamber is now open to cryo pump, and the pressure is further pumped down. When the pressure is down to last 2 decimal places, turn on the ion gauge, and wait till the pressure foes down to 5×10^{-6}.
7. Turn on the power to magnetron drive.
8. Set timer for deposition time (0.4 minutes for 40 nm of Pt).
9. Close the throttle valve and turn gas 1 on.
10. Wait till air flow stabilizes (around 30), and pressure around 60 mT.
11. Turn on DC target selector and select station 4.
12. Turn the power supply on. Deposition power is set to 0.1 KW. Not the stable voltage. Sputter for 1 min, with lid on. Turn on timer and shutter 4 at the same time so that the sample is sputtered for required time.
13. After the deposition turn off power and gas 1 and open throttle valve.
14. Turn off HVAC and hit vent. Wait till the vacuum light is green and use hoist up to open the chamber.
15. Unload the sample carefully and turn the Argon gas off.